

Dispersion Relation Constrained Partial Wave Analysis of πN Elastic and $\pi N \rightarrow \eta N$ Scattering Data: The Baryon Spectrum

R. A. Arndt,^{*} W. J. Briscoe,[†] I. I. Strakovsky,[‡] and R. L. Workman[§]
*Center for Nuclear Studies, Department of Physics,
 The George Washington University, Washington, D.C. 20052, U.S.A.*

M. M. Pavan[¶]
TRIUMF, Vancouver, B.C. V6T 2A3, Canada

We present results from a comprehensive partial-wave analysis of $\pi^\pm p$ elastic scattering and charge-exchange data, covering the region from threshold to 2.1 GeV in the lab pion kinetic energy, employing a coupled-channel formalism to simultaneously fit $\pi^- p \rightarrow \eta n$ data to 0.8 GeV. Our main result, solution FA02, utilizes a complete set of forward and fixed-t dispersion relation constraints, from threshold to 1 GeV, and from $t = 0$ to $-0.4 (GeV/c)^2$, applied to the πN elastic amplitude. A large number of systematic checks have been performed, including fits with no charge-exchange data and other database changes, fits with few or no dispersion relation constraints, and changes to the Coulomb correction scheme. We have also reexamined methods used to extract Breit-Wigner resonance parameters. The quality of fit to both data and dispersion relation constraints is superior to our earlier work. The results of these analyses are compared with previous solutions in terms of their resonance spectra and preferred values for couplings and low-energy parameters, including the πNN coupling constant.

PACS numbers: 14.20.Gk, 13.30.Eg, 13.75.Gx, 11.80.Et

I. INTRODUCTION

The determination of resonance properties for all accessible baryon states is a central objective in Nuclear Physics. Pole positions, decay channels, and branching ratios have been extracted from hadronic reaction data. Further results for magnetic moments and photo-decay amplitudes have been obtained from real and virtual photon interactions. This body of information has been used to test QCD-inspired models and, more recently, lattice calculations.

Most N and Δ resonances, listed as 3- and 4-star states in the Review of Particle Properties (RPP) [1], have had their existence, masses, and widths determined through single-channel fits to scattering data, with πN elastic scattering being the predominant source. Similarly, most photo-decay amplitudes have been determined in fits to single-pion photoproduction. However, a number of recent studies of eta photoproduction and electroproduction data have claimed [2] resonance properties for the $N(1535)$ and $N(1520)$ at variance with these long-standing pion production results. Multi-channel analyses have provided further estimates [3] which also tend to disagree with the single-channel values.

These problems have motivated an improved analysis of πN elastic scattering in the ηN threshold region. Here, we report the results of a coupled-channel fit to πN elastic and ηN production data, the $\pi N \rightarrow \eta N$ data having been incorporated through a Chew-Mandelstam K-matrix formalism [4]. Compared to our previous work (solution SM95 [5]), the present FA02 analysis has fitted a larger database, in particular new high-quality data in the $\Delta(1232)$ resonance region (described in Section II). In addition to the forward $C^\pm(\omega)$ and fixed-t $B^\pm(\nu, t)$ dispersion relation constraints already used in SM95, our new solution has been constrained by further forward derivative $E^\pm(\omega)$ and fixed-t $C^\pm(\nu, t)$ dispersion relations [6] over broader ranges of energy and four-momentum transfer.

In Section III, we will explain how the dispersion relation constraints were implemented. For comparison purposes, fits to the available data were also performed with fewer, and no, dispersion relation constraints. This has helped to

^{*}Electronic address: arndt@reo.ntelos.net

[†]Electronic address: briscoe@gwu.edu

[‡]Electronic address: igor@gwu.edu

[§]Electronic address: rworkman@gwu.edu

[¶]Electronic address: marcello.pavan@triumf.ca

gauge the relative effect of such constraints on the quality of fit to data. Many other fits were performed to study systematic effects on resonance and dispersion relation parameters, in particular the πNN coupling constant. We have performed fits excluding charge-exchange data, employing different datasets in the $\Delta(1232)$ region, using different Coulomb correction schemes, and retaining the older Karlsruhe [7] D-waves at low energies, to gauge the influence of these poorly known amplitudes.

In Section IV A, we compare the present FA02 solution with both our previous SM95 solution and results from previous analyses, as well as giving values for the partial-wave amplitudes. The baryon spectrum, and associated couplings are given in Section IV B, whereas results for the πNN coupling constant and other dispersion relation parameters are discussed in Section IV D. In Section V, we provide a brief summary and consider what extensions of this work can be expected in the future.

II. DATABASE

The evolution of our database is summarized in Table I. Over the course of four previous pion-nucleon analyses [4, 5, 8, 9] our energy range has been extended from 1.1 to 2.1 GeV. Additions to the current database [10] are due mainly to measurements in the low (below 300 MeV) energy region. We have also incorporated 173 η production data (from the process $\pi^- p \rightarrow \eta n$). Below, we list the recent (post-1995) additions for elastic and charge-exchange scattering. The eta-production database, being recently added, contains both new and old measurements. Here, we should note that the full database contains conflicting results. Some of these with very large χ^2 have been excluded from our fits. However, all available data have been retained (the excluded data labeled as “flagged” [11]) so that comparisons can be made through our on-line facility [10]. Some individual data points were also removed from the analysis in order to resolve conflicts or upon authors’ requests (since our previous analysis [5], we have flagged 48 π^+ and 35 π^- data, most of these being total cross sections). Some of the data, listed as new, were available in unpublished form at the time of our previous analysis [5]. A complete description of the database and those data not included in our fits is available from the authors [10]. The energy-angle distribution of recent (post-1995) $\pi^+ p$, $\pi^- p$ elastic, $\pi^- p \rightarrow \pi^0 n$, and all $\pi^- p \rightarrow \eta n$ data is given in Fig. 1.

Since most of the new data [13, 14, 15, 16, 17, 18, 19, 20, 21, 22, 23, 24, 25, 26, 27, 28] are from high-intensity facilities (such as LAMPF, TRIUMF, and PSI), they generally have smaller statistical errors and, thus, have a greater influence on the fits. As mentioned above, a large fraction of the more recent $\pi^\pm p$ data were produced at energies spanning the $\Delta(1232)$ resonance. These data have been taken mainly at TRIUMF. From this source, we have added 106 $\pi^+ p$ and 54 $\pi^- p$ differential cross sections, from 140 to 270 MeV at medium scattering angles [13], and 41 $\pi^+ p$ (37 $\pi^- p$) cross sections, from 90 to 140 MeV [14]. A further 194 $\pi^+ p$ and 81 $\pi^- p A_y$ data between 90 and 280 MeV, at medium and backward scattering angles, have been collected using the CHAOS facility at TRIUMF [15, 16]. At low energies, 55 to 140 MeV, and backward scattering angles, 13 $\pi^+ p$ and 89 $\pi^- p A_y$ data have also become available from CHAOS [17].

A few LAMPF experiments have now been analyzed and added to our database. These include 36 high-quality polarized charge-exchange data between 100 and 210 MeV [19], 40 low-energy (10 to 40 MeV) cross sections [20], and 6 forward charge-exchange differential cross sections at 27 MeV [22].

We have added 23 $\pi^+ p$ and 6 $\pi^- p$ TRIUMF [18] and 44 $\pi^+ p$ and 15 $\pi^- p$ LAMPF [21] partial total cross sections from 40 to 280 MeV [18], though this quantity is not fitted in the analysis.

PSI experiments have provided 5 $\pi^- p$ differential cross sections in the backward hemisphere between 45 and 70 MeV [23] and 11 A_y data at 160 and 240 MeV [24]. After a revised analysis, the Karlsruhe group has published a final set of both $\pi^\pm p$ low-energy differential cross sections [25] and analyzing powers [26].

A set of polarization parameters P , R , and A for both $\pi^+ p$ and $\pi^- p$ from 870 to 1490 MeV were contributed by the ITEP–PNPI Collaboration [27, 28].

In the $\Delta(1232)$ resonance region, there are two sets of data which are in disagreement, primarily on the rising side of the resonance: the first includes the PSI total cross section data of Pedroni *et al.* [29] and the differential cross sections of Brack *et al.* [14, 30], while a second set includes the total cross sections of Carter *et al.* [31] and the differential cross sections of Bussey *et al.* [32]. Since the resonant $\Delta(1232)$ (P_{33}) amplitude dominates most dispersion relations, discrepant data bases in this energy region are no small concern. In our previous solution [5], the Bussey *et al.* data were assigned 5% normalization uncertainties, and the Carter *et al.* data were assigned 1.5% uncertainties, to resolve a discrepancy between the energy-dependent and single-energy solutions. Subsequent to that solution, the normalization uncertainties in the Bussey *et al.* and Carter *et al.* data were reevaluated (to 1%), and the lowest energy measurements in each of the $\pi^+ p$ and $\pi^- p$ total cross sections were removed, by one of the principal authors [33]. The data were so employed in the present solution. However, with the addition of new TRIUMF

differential cross section [13] and polarization data [15, 16], the changes in phases and dispersion relation parameters arising from selecting one of the aforementioned discrepant data sets have greatly diminished, as will be discussed in Sec. IV D. All of the above data sets are included in the fitted database.

Most measurements of the $\pi^-p \rightarrow \eta n$ reaction cross section are rather old and sometimes conflicting. There are few cross section measurements above 800 MeV and no polarized measurements below 1040 MeV [10]. We have selected 138 differential and 35 total cross sections for our analysis, with an additional 176 data points added to the on-line database but not included in this study [34, 35, 36, 37, 38, 39, 40, 41, 42, 43, 44, 45, 46]. A detailed analysis of the older data can be found in the review by Clajus and Nefkens [47]. Previous unpolarized measurements are listed in Ref. [48]. One new set [34] of data has been included in our analysis. Total and differential cross sections for $\pi^-p \rightarrow \eta n$, near threshold, were measured using the BNL-AGS Facility [34]. Cross sections were obtained from threshold (560 MeV) to ~ 650 MeV with $\sim 10\%$ statistics for the total cross sections. The angular coverage was $45\text{--}155^\circ$. Systematic uncertainties were estimated at $\sim 3\%$, a value significantly less than claimed in previous measurements, where systematics were above 10%.

III. FORMALISM

There are three principal components to the methodology we use in fitting πN elastic scattering, charge exchange and $\pi^-p \rightarrow \eta n$ data: (i) the energy-dependent parametrization of partial waves, (ii) dispersion-relation constraints, and (iii) Coulomb interaction effects.

A. Chew-Mandelstam K-matrix

Our energy-dependent partial-wave fits are parameterized in terms of a coupled-channel Chew-Mandelstam K-matrix, as described in Refs. [4, 5]. This choice determines the way we introduce and modify the energy-dependence and account for unitarity in our fits.

The scattering into different channels is represented by a matrix \bar{T} , parameterized in terms of \bar{K} , a (4×4) real symmetric K-matrix for each partial wave

$$\bar{T} = \bar{K}(1 - C\bar{K})^{-1}, \quad (1)$$

C being a diagonal Chew-Mandelstam function, with $\text{Im}C_i = \rho_i$ giving the phase-space function for the i^{th} channel (πN , ηN , $\pi\Delta$, and ρN). The T-matrix for elastic πN scattering is then given by $T_{\pi\pi} = \bar{T}_{\pi\pi}\rho_\pi$; for $\pi N \rightarrow \eta N$, the relation being $T_{\pi\eta} = \bar{T}_{\pi\eta}(\rho_\pi\rho_\eta)^{1/2}$. The ρN channel is new to the present solution. Its inclusion has reduced the number of parameters by 6, compared to SM95 [5], while improving the fits and dispersion relation consistency (the ρ width is accounted for in this approach). It should be noted that the above $\pi\Delta$ and ρN channels are generic and included to preserve unitarity. Unlike the SM95 fit, however, the ηN channel has been fitted to physical cross sections.

In order to control the behavior of each T-matrix near threshold, the K-matrix elements were expanded as polynomials in the energy variable $Z = (W - W_{th})$, where W and W_{th} are the center-of-mass (\sqrt{s}) and threshold energies, respectively. Multiplying by an added factor of Z allowed the fixing of scattering lengths through the value of the leading term.

Single-energy analyses were parametrized as

$$S_e = (1 + 2iT_e) = \cos(\rho) e^{2i\delta}, \quad (2)$$

with the phase parameters δ and ρ expanded as linear functions around the analysis energy, and with a slope (energy derivative) fixed by the energy-dependent solution. It should be emphasized that the single-energy solutions are generated mainly to search for missing structure. The scatter around an energy-dependent solution is also useful as a measure of the uncertainty in a partial wave. The variation from point-to-point should not be taken as proof of sharp structures, as these binned fits are far less constrained than the global fits (they do not, for example, satisfy the dispersion relation constraints) [49].

Threshold behavior was determined in the following manner. The S-wave scattering lengths were linked to our dispersion relation constraints, as described below. The P-wave scattering volumes were searched without constraint, but it was ensured that near threshold these waves followed the appropriate Chew-Low forms [50, 51], which are approximations to the respective partial-wave dispersion relations. The D-waves were weakly constrained to the older Karlsruhe analysis by assigning 5% errors to the Koch values [7], and the low-energy behavior of higher waves was

fixed to Koch's result [7]. Once an appropriate hadronic amplitude was determined, charge corrections were applied as described in Sec. III C.

B. Dispersion Relation Constraints

In general, a fit of the K-matrix elements, expanded in terms of an energy variable, may not result in a form satisfying all of the requirements imposed by analyticity and crossing symmetry. In our analysis, those requirements are addressed at fixed four-momentum transfer t by a complete set of fixed- t dispersion relations (DRs), which are handled iteratively with the data fitting, as has been described in Ref. [5]. The DRs contain subtraction constants which should be independent of energy (but which can be functions of four-momentum transfer). After each data-fitting iteration, these constants are calculated as a function of energy. χ^2 deviations from the average, at a series of energies, are then calculated and included as pseudo-data. Figure 2 shows an example of the subtraction constants in the forward $C^\pm(\omega)$ DRs up to 1 GeV, ω being the pion lab energy. The partial-wave amplitudes and the real parts of the DR invariant amplitudes are then adjusted to minimize the χ^2 from the sum of data and pseudo-data. Compatibility with the DR constraints can be controlled through the errors assigned to pseudo-data in the fit.

In our previous published analysis [5], we employed constraints from fixed- t DRs for the $B_\pm(\nu, t)$, ν equal to $(s - u)/4M$, and forward $C^\pm(\omega)$, invariant amplitudes [52]. Constraints on the partial-wave fits were generated at fixed values of t ranging from 0 to $-0.3 (GeV/c)^2$ and pion lab kinetic energies from 25 to 600 MeV. The $B_\pm(\nu, t)$ DRs were constructed in the Hüper form [6]. The full πN amplitude was parameterized by two invariant amplitudes $B^\pm(\nu, t)$ and $C^\pm(\nu, t)$ (or equivalently $B^\pm(\nu, t)$ and $A^\pm(\nu, t)$). While in the analysis of Ref. [5] the C^\pm amplitudes were reasonably well behaved, improvement called for their inclusion in DR constraints at non-forward angles.

With the inclusion of constraints from the fixed- t $C^\pm(\nu, t)$ DRs, we complete the fixed- t DRs coverage of the full πN amplitude. The C^\pm DRs were chosen since parameterizations of the very high energy amplitudes are readily available [6]. The energy and four-momentum transfer coverage was increased for most fixed- t DRs to $T_\pi < 1000$ MeV and $0 \leq -t \leq 0.4 (GeV/c)^2$. This t range covers the entire angular range up to ~ 450 MeV, across the important $\Delta(1232)$ resonance region, which contains the most accurate and complete data sets. Due to use of analytically smooth energy-dependent amplitudes, the DRs are approximately satisfied over wider constraint energy and t ranges (see results in Section IV D).

In addition to the fixed- t $C^\pm(\nu, t)$ DRs, the present analysis includes constraints from the forward derivative DRs

$$E^\pm(\omega) = \frac{\partial}{\partial t} [A^\pm(\nu, t) + \omega B^\pm(\nu, t)]|_{t=0} \quad (3)$$

utilized in Ref. [53]. These DRs were also applied from $10 < T_\pi < 1000$ MeV. The $E^\pm(\omega)$ DRs provide a stronger constraint on higher partial waves, which are more poorly known at low energies. Nevertheless, the $l = 1$ $\Delta(1232)$ resonance gives a dominant contribution, as is the case for most of the other DRs we employ. Consistency of the fixed- t $C^\pm(\nu, t)$ DRs is illustrated in Fig. 3. As in Fig. 2, the plotted constant is obtained through a delicate cancellation between pole contributions and principal value integrals. The variation of these contributions is displayed for the forward $E^\pm(\omega)$ DRs in Fig. 4.

Dispersion relations contain principal value integrals over the imaginary parts of invariant amplitudes up to infinite energy. The subtraction constants are used to ensure convergence of these integrals. As our analysis extends up to 2100 MeV, the amplitudes above this energy are obtained from other sources. For the energy region 2100–5000 MeV, the Karlsruhe KA84 πN analysis solution [54] is utilized. At higher energies, parameterizations were taken from Ref. [6]. These high-energy contributions are relatively small for the Hüper DR and isovector amplitudes, but are important for the isoscalar E^+ and C^+ amplitudes. In these latter cases, while high-energy contributions were necessary to achieve sufficient convergence, the various forms of parameterization [6] yielded negligible differences in the DR constraints.

As mentioned above, DRs contain a number of parameters which are *a priori* unknown, namely the various subtraction constants (if inserted for convergence of the DR integrals) and the πNN coupling constant $g^2/4\pi$ (when the Born term appears). These constants are considered free parameters to be determined from the fits to the data and the DR constraints. In principle, these subtraction constants can be determined at any energy. We fix them at the physical threshold for the forward DRs, and at the unphysical points $C^\pm(0, t)$ for the fixed- t C^\pm DRs. The former can be expressed in terms of the S-wave scattering lengths a^\pm (C^\pm DRs) and the P-wave scattering volumes a_{1+}^\pm (E^\pm DRs).

These parameters could be determined in a number of ways. In the present study, we settled on the following procedure: for a particular DR and data minimization run, the $\pi^- p$ S-wave scattering length a_- was fixed around

precise results extracted from the PSI pionic-atom experiment [55], and the coupling constant $g^2/4\pi$ and scattering volume a_{1+}^+ were fixed at chosen values. In essence, the π^-p S-wave scattering length a_- is used as an additional data point at threshold. The other parameters (including the isovector S-wave scattering length a^-) were allowed to float freely. As a result, the subtraction constant was fixed for the forward C^+ and E^+ DRs, with real parts of the amplitudes forced to particular values in the analysis, whereas analogous constants for the other DRs were allowed to find their own level. Once a solution with minimal χ^2 was determined, further runs were performed with new sets of fixed $(g^2/4\pi, a_{1+}^+)$ values, producing a mapping over a grid of parameters. The solution FA02 was selected from this grid of solutions based on overall χ^2 .

Generally, the χ^2 variation of parameters is parabolic in the region near a minimum. The advantage of a grid method is that the depth of the $(g^2/4\pi, a_{1+}^+)$ minimum in χ^2 space indicates how well these parameters are determined. One can also view the dependence of the χ^2 in each πN charge channel, or the DR pseudo-data, separately to look for systematic variations.

We found the mapping procedure to be necessary for $(g^2/4\pi, a_{1+}^+)$ due to computational instabilities which arise occasionally. One could, in principle, fix all the parameters and follow the above procedure over a multi-dimensional grid, and tests were done to investigate this, but it was found that the above procedure was sufficient to ensure stable fits with well-satisfied DRs in all cases, while keeping the χ^2 fit to the data optimal. Adding more, or fixing more constraints, increases the data fit χ^2 .

C. Coulomb Interaction

The partial-wave and DR analyses are performed using purely isospin-conserving hadronic amplitudes, so Coulomb and other isospin-violating contributions must be introduced before constructing observables to compare to the physical pion-proton scattering data. There is no unique way to split the interaction into strong and electromagnetic parts [56], so in general models must be used.

In previous analyses, we have used a simple point-source barrier factor correction for all partial waves at all energies, as discussed in Ref. [4]. The main isospin-violating contribution is the $\Delta^{++} - \Delta^0$ mass and width difference, which we have been treating phenomenologically by splitting the average resonant hadronic P_{33} partial-wave into P_{33}^+ and P_{33}^- waves for π^+p and π^-p , respectively. The Δ mass and width differences were found from a best fit to the data. A further correction was made to the P_{33} amplitude to account for the $\pi^-p \rightarrow \gamma n$ channel. The mass ($\Delta^0 - \Delta^{++}$) and width ($\Gamma^0 - \Gamma^{++}$) differences are 1.74 ± 0.15 MeV and 1.09 ± 0.64 MeV, respectively [57].

The main criticism of point-source barrier factors is that they exaggerate the S-wave corrections at low energies, since the $l = 0$ partial waves do not vanish at the origin, while the point-Coulomb field diverges there. Consequently, in this study, we have used the Nordita [58] Coulomb prescription, which was used for the Karlsruhe-Helsinki (KH80) analyses [59]. However, the Nordita work supplied corrections for only the largest S- and P-waves up to 530 MeV, whereas our analysis extends to 2100 MeV. The Nordita corrections were therefore supplemented with corrections calculated from Gibbs extended-source barrier factors [60] for S- and P- waves at energies above 450 MeV, and D- and higher waves at all energies. The Nordita and Gibbs results were smoothly joined in the 450 MeV region. As well, an error was found and corrected in the isospin mixing term in one Nordita source [58], while the pure Coulomb part of the (dominant) resonant P_{33} correction was reduced 15% to take into account intermediate σ exchange [61], which was missing in the Nordita work.

The Nordita corrections already contain effects due to the $\pi^+ - \pi^0$ mass difference. In this scheme, the π^+ channel corresponds to the hadronic channel, and all isospin violating effects (due to mass differences and the γn channel) are subsumed in the π^- amplitudes. To remain consistent with this scheme, we have redefined our $\Delta(1232)$ resonance charge-splitting analogously. This has had the effect of shifting the peak of the hadronic resonance to a slightly lower energy.

Final FA02 Coulomb correction results for the S_{31} and P_{33} partial-wave are plotted in Fig. 5, along with the point-source barrier factor results. Differences between the FA02 and point-source corrections (not shown) are similarly large in the S_{11} partial-wave, as expected, while for all other waves, the differences are much smaller. However, these differences in the SM95 and FA02 correction schemes did not result in large effects on the fits or dispersion relation parameters.

IV. RESULTS AND DISCUSSION

A. FA02 versus the SM95 Fit

The main result of this work has been an energy-dependent solution (FA02) having a χ^2 of 45874 for 23979 (π^\pm elastic, with pion induced π^0 and η production) data to 2.1 GeV (η N data have been included to 800 MeV). The overall χ^2/data was significantly lower than that found in our previously published fit ($\chi^2/\text{data} = 2.2$) [5], despite the inclusion of additional data. This change is partly a reflection of the database changes mentioned in Section II. Our present and previous energy-dependent solutions are compared in Table I. As in previous analyses, we have used the systematic uncertainty as an overall normalization factor for angular distributions. For total cross sections and excitation data, we have combined statistical and systematic uncertainties in quadrature. This renormalization freedom allows a significant improvement in our best-fit results, as shown in Table II. In cases where the systematic uncertainty varies with angle, this procedure may be considered a first approximation.

In Table III, we compare the energy-dependent and single-energy results over the energy bins used in these single-energy analyses. Also listed is the number of parameters varied in each single-energy solution. A total of 172 (94 for isospin 1/2 and 78 for isospin 3/2) parameters were varied in the energy-dependent analysis FA02. The extended database has allowed an increase in the number of single-energy values versus our previous result [5] over the same energy range.

Figs. 6 and 7 compare the energy-dependent fits FA02 and SM95 over the full energy region. Partial waves with $l < 6$ are displayed, whereas the analysis has fitted waves up to $l = 6$. Deviations from SM95 are visible in amplitudes S and P for $I = 1/2$, and the D waves, mainly near the end point of our analysis. Considering the complicated structure associated with an opening η n channel and N(1535) resonance, the S_{11} partial-wave shows remarkably little deviation from the earlier SM95 fit.

B. Resonance Parameter Extraction

The resonance spectrum from our fit has been extracted using three different methods. Poles and zeros have been found by continuing into the complex energy plane. These are compiled in Tables VI, VII, and VIII along with the modulus and phase of all pole residues. The complicated interplay of poles and zeros is displayed in Fig. 8 for the S_{11} and P_{11} partial waves. Clearly, for these partial waves and their associated resonances, a simple Breit-Wigner parameterization should be avoided. An error in the routine used to determine pole residues for SM95 was found [62] and corrected. The most significant change is seen in the $\Delta(1232)$ residue, which now agrees with most previous determinations.

More commonly used, though more model-dependent, are Breit-Wigner parameters for the resonances. Here, as for the SM95 fit, a Breit-Wigner plus background contribution was initially fitted to the single-energy amplitudes, over varying ranges of energy. However, given the scatter often found in the single-energy values, we have rejected this method in favor of another. In Tables IV and V, we give resonance parameters obtained from a Breit-Wigner plus background (using a product S-matrix approach, $S = S_R S_B$) representation applied directly to the data. Here, $S_R = 1 + 2i T_R$, with

$$T_R = \frac{\Gamma_\pi/2}{W_R - W - i(\Gamma_\pi/2 + \Gamma_I/2)}. \quad (4)$$

The total width is given by $\Gamma = \Gamma_\pi + \Gamma_I$, where

$$\Gamma_\pi = \rho_\pi \Gamma R, \quad (5)$$

$$\Gamma_I = \rho_i \Gamma (1 - R),$$

with R being the branching fraction to π N. The background T-matrix is given in terms of a K-matrix, $T_B = K_B(1 - iK_B)^{-1}$, with $K_B = A + B(W - W_R) + iC$. Only one background parameter was necessary for the $I = 3/2$ waves. Data were then fitted using this representation for a particular resonant partial wave. The remaining waves were fixed to values found in the full global analysis. Values for the background parameters, energy ranges over which fits were performed, and χ^2 comparisons are given in Tables IX and X. In Fig. 9, S-, P-, D-, and F-wave resonances are compared in terms of their pole positions versus a fitted Breit-Wigner mass and width.

In Table IV, results for the N(1535) and N(1650) resonances are significantly different than those reported in the SM95 analysis. The widths of both states are now closer to their RPP averages. The N(1650) continues to show a nearly elastic behavior in the FA02 solution. This structure also appears to be difficult to parameterize, requiring the most background parameters in the present representation. Breit-Wigner parameters are absent for the $\Delta(1920)$ as this fit produces a mass about 500 MeV greater than suggested by the pole position.

In Table XI, we give resonance parameters determined from a fit to data without DR constraints. In most cases, there is reasonable agreement with the constrained fit. An exceptions appears to be the $P_{13}(1720)$, which has a relatively weak coupling to πN states, and has an atypical resonance signature.

C. Charge-Symmetry Violation in πN Scattering

The issue of charge symmetry violation (CSV) is fundamental to our understanding of hadronic interactions, and many experimental and theoretical studies have addressed this issue (see review [63]). In the framework of QCD, CSV arises from the mass difference between the u and d quarks. The other principal cause for CSV comes from the electromagnetic interaction, as described in Sec. III C. Weinberg [64] pointed out that the effective chiral πN Lagrangian, coming from QCD, contains a term which violates charge symmetry (see also, a recent review by Meissner [65]). Thus, not only are there kinematic reasons for CSV due to the mass differences within baryon multiplets, but direct CSV effects should exist as well. Recent analyzes [66, 67] of the triangle identity in low-energy πN scattering (below 70 MeV) data have found some indications for significant (6-7%) direct CSV effects in the strong-interaction sector [66, 67]. Fettes and Meissner [68] have found a somewhat smaller violation ($\sim 2.5\%$) in a third order chiral perturbation theory calculation without electromagnetic effects, and even smaller violations once the latter were included [69].

Because our formalism does not employ CSV beyond the Coulomb interaction, which we take into account in our treatment of the database, we have generated a test fit (X370) of the full database excluding charge-exchange data. Differences between FA02 and X370 are therefore signal incompatibilities between the elastic and charge-exchange data, which could be an indication of CSV.

In Table XII, we compare the FA02 and X370 solutions. For the energy range associated with meson factories (below 500 MeV), there is little difference between FA02 and X370. Above 500 MeV, a significant χ^2 contribution comes from the old Rutherford High Energy Laboratory (RHEL) $\pi^+ p$ P measurements where there are 1976 P data from 480 to 2080 MeV [70] favoring by $\chi^2 \sim 200$ the fit X370 versus FA02. Conversely, for charge-exchange $d\sigma/d\Omega$ two old RHEL sets (416 cross sections from 900 to 2050 MeV [46], 156 backward cross sections from 480 to 870 MeV [37], and one KEK set (72 cross sections from 1830 to 2040 MeV [71]) are more poorly represented, by $\chi^2 \sim 1900$, in X370 versus FA02. At very low energies, there exist rather few charge-exchange data, and almost no polarization data, so a precise test of the Fettes and Meissner [68, 69] prediction is not possible. As a result, we cannot claim any compelling evidence for sizable CSV effects in πN elastic scattering. This is consistent with recent findings for $\pi 2N$ and $\pi 3N$ systems [72].

D. Dispersion Relation Parameters

Results for the forward $C^\pm(\omega)$, forward derivative $E^\pm(\omega)$, and fixed- t $C^\pm(\nu, t)$, Hüper, and $B^+(\nu, t)$ DRs are summarized graphically in Figures 2 – 4, 10, and 11, respectively. The form of $B^+(\nu, t)$ DR displayed in Fig. 4 was used in Ref. [73] in a determination of the coupling constant. This form was not used as a constraint in FA02, but is included here for its utility in illustrating the uncertainty associated with $g^2/4\pi$. These DRs are well satisfied over the whole constraint region up to a kinetic energy $T_\pi = 1$ GeV and a four-momentum transfer $t = -0.4$ (GeV/c)². The consistency of FA02 with these constraints is much better than our previous solution SM95 [5] and the solutions KA84 [54] and KH80 [59]. Due to the energy-dependent parameterization of our partial waves, all fixed- t DRs are well satisfied up to $t = -0.5$ (GeV/c)², with all isovector DRs reasonably well satisfied up to ~ 2 GeV *i.e.* the entire data range. The more sensitive isoscalar DRs remain reasonably well satisfied up to 1100–1300 MeV; constraints for the forward $C^+(\omega)$ DR extended to 0.8 GeV.

Figure 12 compares the “Chew-Low” [50] and scattering length (volume) plots for the FA02 and Karlsruhe [54] S- and P-wave amplitudes. Exact agreement with the values given in Fig.2 is not expected, as the method is different. The FA02 Chew-Low plots have a very similar behavior to the partial-wave dispersion relation (PWDR) constrained KA84 solution. This indicates that FA02 at least approximately satisfies a P-wave PWDR. The present solution fixes a long-standing discrepancy in the P_{13} Chew-Low behavior observed in our previous solutions [5, 8, 9].

The present solution FA02 yields the DR parameters $g^2/4\pi = 13.75 \pm 0.10$ for the pion-nucleon coupling constant, $a_{1+}^+ = 0.133 \pm 0.001 \mu^{-3}$ ($a_{1+}^- = -0.074 \pm 0.001 \mu^{-3}$) for the P-wave scattering volumes, and $3a_{0+}^- = 0.2650 \pm 0.0014 \mu^{-1}$ and $a_{\pi^-p} = 0.0870 \pm 0.0013 \mu^{-1}$ (implying $a_{0+}^+ = -0.0010 \pm 0.0012 \mu^{-1}$) for the S-wave scattering lengths. The coupling constant confirms our earlier result in Ref. [5] and is in line with other determinations [74, 75]. The scattering lengths are in agreement with those of the PSI pionic-hydrogen and pionic-deuterium experiments [55].

Our DR procedure constrains the π^-p scattering length to *agree* (within some error bound) with the result from the PSI pionic-atom experiment [55] ($a_{\pi^-p} = 0.0883 \pm 0.0008 \mu^{-1}$), so the above agreement in a_{π^-p} is not surprising. However, a solution constructed to be otherwise identical to FA02, but where a_{π^-p} was *not* constrained to the PSI value, yielded a best fit with $a_{\pi^-p} = 0.0856 \pm 0.0010 \mu^{-1}$, indicating the value sought by the scattering data alone. Consequently, a compromise value of ~ 0.087 a little lower than the PSI result was chosen as the constraint value for FA02. Ericson, Loiseau, and Wycech have published [76] a reanalysis of the PSI result [55], and have obtained $a_{0+}^- = 0.0883 \pm 0.0027 \mu^{-1}$ and $a_{\pi^-p} = 0.0870 \pm 0.0005 \mu^{-1}$, the latter reasonably consistent with our result $0.0856 \pm 0.0010 \mu^{-1}$ using data alone.

The systematic check described above is one of many that we have applied to our solution. A large number of test solutions were obtained with varying fitting and constraint conditions, to investigate systematic uncertainties in the extracted DR parameters. These systematics checks are discussed in detail below.

- A solution (P370) using the point-Coulomb corrections employed in our previous solutions Refs. [5, 8, 9] gave an overall χ^2 fit very similar to FA02. Differences in the resulting parameters were not large. For $g^2/4\pi$ and a_{0+}^- , this solution gave 13.69 and $0.0867 \mu^{-1}$, respectively. Despite seemingly large differences between the point-Coulomb and Nordita+Gibbs [58, 60] schemes (see Fig. 5), the consistency of results indicates that our Coulomb correction scheme is adequate to perform this type of partial-wave analysis.
- In an isospin-invariant framework, charge-exchange data are not required to reconstruct the amplitudes. As discussed in Sec. IV C, a solution was constructed (X370) after charge-exchange data were removed from the fitted database. Despite this drastic change, the resulting DR parameters were quite consistent with those of FA02.
- A less drastic change in the database was investigated in the region of the $\Delta(1232)$ resonance. The issue of discrepant data sets on the rising part of the resonance was discussed in Sec. II. To quantify this effect, solutions were constructed employing the data sets of Pedroni *et al.* [29], Brack *et al.* [14, 30], and Pavan *et al.* [13], while floating (applying a normalization error of 100%) those of Bussey *et al.* [32] and Carter *et al.* [31], and vice versa. The π^-p scattering-length constraint was held constant in both cases. The resulting solutions differed in the coupling constant by $\Delta g^2/4\pi = 0.07$, while the scattering lengths remained consistent. Since FA02 fits all the aforementioned data sets together, an uncertainty of ± 0.04 was ascribed to this systematic effect.
- The DR constraints for the FA02 solution were applied up to 1 GeV, and from $t = 0$ to $-0.4 (GeV/c)^2$. Solutions constructed with a reduced range of 25 to 600 MeV and t to $-0.3 (GeV/c)^2$ again yielded results consistent with FA02, the latter ranges having been employed in solution SM95 [5].
- Dispersion relation constraints were both strengthened and weakened by a factor of 2, yielding results consistent with FA02. It should be noted, however, that constraining too tightly yields a very large data χ^2 and numerically unstable fits.
- In addition to the above test, a solution was constructed employing *no* DR constraints. Here, the fit to data was naturally much better than in FA02, but the improvement was less dramatic ($\Delta\chi^2 = 1036$ for 21808 data points) than one might expect, with little difference obvious in a plot of the partial waves. The numerically sensitive C^+ and E^+ isoscalar dispersion relations were understandably not well satisfied; however, the less sensitive C^- and E^- isovector dispersion relations remained rather well satisfied over the full energy range, as were the Hüper and $B^+(\nu, t)$ relations up to ~ 800 MeV and $t = -0.3 (GeV/c)^2$. The extracted constants were $a_{0+}^- = 0.086 \mu^{-1}$, $a_{1+}^- = -0.073 \mu^{-3}$, and $g^2/4\pi = 13.62$.
- The D-waves below ~ 250 MeV are too small to be accurately determined from fits to data alone. The forward derivative E^\pm DRs have an enhanced sensitivity to higher partial waves ($\sim l^3$) and so help to constrain the D-waves. To test the dependence of the DR parameters on these low energy D-waves, a solution was constructed identical to FA02 except constrained rigorously (1%, compared to 5% for FA02) to the low energy Koch D-wave results [7]. The DR parameters changed minimally, the largest changes being 0.002 for both Δa_{1+}^+ , and Δa_{1+}^0 . However, the data χ^2 was increased both above 400 MeV ($\Delta\chi^2 = \sim 600$) and below by ~ 200 , with an increase of ~ 300 in the fit to DR pseudo-data constraints. The fit thus exhibits a clear preference for the FA02 D-waves.

The central values and uncertainties of the DR parameters have been estimated, taking into consideration the systematic checks outlined above, and from other checks within the FA02 solution itself. These include differences in parameter values at the χ^2 minima for each of the charge channels and the DR pseudo-data. For the coupling constant $g^2/4\pi$, we also considered differences in the value extracted from the Hüper (Fig. 10) and $B^+(\nu, t)$ (Fig. 11) dispersion relations, which, along with the database changes around the $\Delta(1232)$, were the dominant sources of uncertainty. The statistical uncertainty stemming from $\Delta\chi^2 = 1$ variations from the minima is negligible compared to systematic effects.

These tests for systematic effects improve our confidence in the values of parameters extracted from FA02. It should be noted, however, that the scattering lengths are tied to the PSI pionic-atom value for the π^-p scattering length. A new more precise experiment is planned [77], and if the result were to change several standard deviations from the present value, this would necessitate a re-analysis. Nonetheless, the value of the pion-nucleon coupling constant would not be expected to change, as it is observed to be robust with respect to modest changes in the π^-p scattering length.

E. The $\pi^-p \rightarrow \eta n$ Channel

Our fit to a representative set of $\pi^-p \rightarrow \eta n$ cross sections is displayed in Fig. 13. In general, over this region, our results are qualitatively similar to other recent multi-channel analyses which have included additional reaction data [3]. Compared to the πN elastic result, the overall χ^2 for this channel is slightly higher. However, we feel this is largely due to problems in the database.

Our coupled-channel approach allows the determination of a number of amplitudes related to the ηN interaction. Fig. 14 gives an Argand [78] plot representation of the energy-dependent fit FA02 over the energy region including $\pi^-p \rightarrow \eta n$ data. Fig. 15 gives a more detailed view of our πN elastic and $\pi N \rightarrow \eta N$ results for the S_{11} and D_{13} partial waves.

V. SUMMARY AND CONCLUSION

We have fitted the existing πN elastic scattering database, employing a complete set of DR constraints, up to $T_\pi = 1$ GeV and $t = -0.4$ (GeV/c)². Data from the reaction $\pi^-p \rightarrow \eta n$ have been included for the first time in an analysis of this type. These improvements have allowed us to more carefully examine the N(1535), which is nearly obscured (in the πN elastic reaction) by the opening of the ηN threshold. Remarkably, the resulting S_{11} partial wave shows little change over this energy region. However, the N(1535) resonance width has changed (increased) dramatically, this being due mainly to our new method for fitting Breit-Wigner parameters. This result should be taken into account by any multi-channel analysis which fits single-energy partial-wave amplitudes.

Our fits without DR constraints and without charge-exchange data have also yielded interesting results. In most cases, an extensive use of DRs had little effect on the extracted resonance spectrum. For weak or non-canonical structures, however, dispersion relations may play a more important role.

In the absence of charge symmetry violation (CSV), beyond Coulomb effects, one should be able to predict the charge-exchange observables based on a fit to elastic scattering data. In the low-energy region, where CSV effects are expected to be most important, our fit excluding charge-exchange data is reasonably predictive, and could be useful in a more refined study of this issue.

An extensive list of tests designed to check for systematic effects (changes to the database, Coulomb-correction scheme) has (a) revealed the DR parameters to be fairly robust with respect to these effects, and (b) suggested a way to quantify these systematic uncertainties. As the FA02 the solution exhibits good consistency with the complete set of forward and fixed- t DRs, we have added confidence in our results. In particular, the πNN coupling has remained quite stable, changing little from our SM95 determination. Our DR analysis and systematic checks will next be applied to an extraction of the nucleon σ -term (see, *e.g.* Ref. [53]). The extraction of this quantity is sensitive to the fine details of the analysis, and a careful examination of the σ -term is in preparation.

Acknowledgments

The authors express their gratitude to B. Bassalleck, V. S. Bekrenev, J. T. Brack, M. Clajus, H. Crannel, J. Comfort, E. Friedman, G. J. Hofman, C. V. Gaulard, L. D. Isenhover, M. Janousch, G. Jones, V. P. Kanavets, M. A. Kovash,

N. Kozlenko, A. A. Kulbardin, I. V. Lopatin, M. Mikuz, R. Meier, V. E. Markushin, T. W. Morrison, D. Počanić, R. A. Ristinen, M. E. Sadler, G. R. Smith, V. V. Sumachev, P. Weber, and R. Wieser for providing experimental data prior to publication or for clarification of information already published. We are grateful to W. R. Gibbs for providing us with a calculation of finite-source-size Coulomb barrier corrections. We also acknowledge useful communications over the years with G. Höhler, D. V. Bugg, and D. M. Manley. This work was supported in part by the U. S. Department of Energy under Grant DE-FG02-99ER41110. The authors (R. A., I. S., and R. W.) acknowledge partial support from Jefferson Lab and the Southeastern Universities Research Association under DOE contract DE-AC05-84ER40150.

-
- [1] K. Hagiwara *et al.* *Review of Particle Physics*, Phys. Rev. D **66**, 010001 (2002); <http://pdg.lbl.gov>.
- [2] See for example, W. T. Chiang, S. N. Yang, L. Tiator, and D. Drechsel, Nucl. Phys. **A700**, 429 (2002) [Eprint nucl-th/0110034]; L. Tiator, D. Drechsel, G. Knöchlein, and C. Bennhold, Phys. Rev. C **60**, 035210 (1999) [Eprint nucl-th/9902028].
- [3] G. Penner and U. Mosel, Phys. Rev. C **66**, 055212 (2002)[Eprint nucl-th/0207069]; T. P. Vrana, S. A. Dytman, and T. S. H. Lee, Phys. Rept. **328**, 181 (2000) [Eprint nucl-th/9910012]; D. M. Manley and E. M. Saleski, Phys. Rev. D **45**, 4002 (1992).
- [4] R. A. Arndt, J. M. Ford, and L. D. Roper, Phys. Rev. D **32**, 1085 (1985).
- [5] R. A. Arndt, I. I. Strakovsky, R. L. Workman, and M. M. Pavan, Phys. Rev. C **52**, 2120 (1995) [nucl-th/9505040].
- [6] G. Höhler, *Pion-Nucleon Scattering*, Landoldt-Börnstein Vol. **I/9b2**, edited by H. Schopper (Springer Verlag, 1983).
- [7] R. Koch, Nucl. Phys. **A448**, 707 (1986).
- [8] R. A. Arndt, R. L. Workman, and M. M. Pavan, Phys. Rev. C **49**, 2729 (1994).
- [9] R. A. Arndt, L. Zhujun, L. D. Roper, R. L. Workman, and J. M. Ford, Phys. Rev. D **43**, 2131 (1991).
- [10] The full database and numerous PWAs can be accessed via an ssh call to the SAID facility gwdac.phys.gwu.edu, with userid: said (no password), or a link to the website <http://gwdac.phys.gwu.edu>.
- [11] The 1-, 2-, and 3-star rating of data is described in Ref. [9]. Only 2- and 3-star data are included in analyses. Unrated data are included unless they have been “flagged” for deletion from analyses. It should be noted that these flagged data are still retained in our database. We have followed this recipe since 1990 [12].
- [12] Historically, B. M. K. Nefkens, W. J. Briscoe, M. M. Sadler, R. A. Arndt, and G. Höhler analysed and classified all πN measurements completed before 1983. 0-, 1-, 2-, and 3-star ratings were assigned to the πN database entries. This star rating system was described at Few Body’83 and the 1st πN International Workshop by B. M. K. Nefkens, in [*Few Body Problems in Physics (Contr. Papers) (Proceedings of 10th International Conference on Few Body Problems in Physics, Karlsruhe, Germany, 1983)*] edited by B. Zeitnitz, 1984, p. 137; Nucl. Phys. **A416**, 193 (1984); Proceedings of the First Workshop on πN scattering, Karlsruhe, Germany, Aug. 1984, edited by G. Höhler].
- [13] M. M. Pavan, J. T. Brack, F. Duncan, A. Feltham, G. Jones, J. Lange, K. J. Raywood, M. E. Sevier, R. Adams, D. F. Ottewell, G. R. Smith, B. Wells, R. L. Helmer, E. L. Mathie, R. Tacik, R. A. Ristinen, I. I. Strakovsky, and H-M. Staudenmaier, Phys. Rev. C **64**, 064611 (2001) [nucl-ex/0103006].
- [14] J. T. Brack, P. A. Amaudruz, D. F. Ottewell, G. R. Smith, M. Kermani, M. Pavan, D. Vetterli, R. A. Ristinen, S. Høibråten, M. D. Kohler, J. J. Kraushaar, B. J. Kriss, J. Jaki, M. Metzler, and E. F. Gibson, Phys. Rev. C **51**, 929 (1995). We used these data in the SM95 analysis [5].
- [15] G. J. Hofman, G. R. Smith, T. Ambardar, F. Bonutti, J. T. Brack, P. Camerini, J. Clark, P. P. J. Delheij, F. Farzanpay, L. Felawka, E. Fragiaco, E. F. Gibson, J. Graeter, N. Grion, M. Kermani, E. L. Mathie, R. Meier, D. Ottewell, R. J. Peterson, R. A. Ristinen, R. Rui, M. E. Sevier, H. Staudenmaier, R. Tacik, and G. J. Wagner, Phys. Rev. C **58**, 3484 (1998).
- [16] G. J. Hofman, J. Breitschopf, K. Craig, H. Denz, E. F. Gibson, E. L. Mathie, R. Meier, M. M. Pavan, C. M. Riedel, R. Tacik, and G. J. Wagner, Phys. Rev. C **68**, 018202 (2003).
- [17] J. D. Patterson, G. J. Hofman, J. T. Brack, P. Camerini, J. Clark, P. P. J. Delheij, L. Felawka, E. Fragiaco, E. F. Gibson, N. Grion, B. Jamieson, E. L. Mathie, R. Meier, D. Ottewell, R. J. Peterson, K. Raywood, R. A. Ristinen, R. Rui, M. E. Sevier, G. R. Smith, R. Tacik, G. Tagliente, G. J. Wagner, and D. M. Yeomans, Phys. Rev. C **66**, 025207 (2002).
- [18] E. Friedman, A. Goldring, G. J. Wagner, A. Altman, R. R. Johnson, O. Meirav, and B. K. Jennings, Nucl. Phys. **A514**, 601 (1990); M. M. Pavan, in *Proceedings of 6th International Symposium on Meson-Nucleon Physics and the structure of the nucleon, Blaubeuren/Tübingen, Germany, July 1995*, edited by G. J. Wagner, R. Bilger, and T. Hehl, πN Newsletter **11**, 117 (1995); E. Friedman, private communication, 1996.
- [19] C. V. Gaulard, C. M. Riedel, J. R. Comfort, J. F. Amann, M. E. Beddo, R. L. Boudrie, G. R. Burleson, P. L. Cole, K. K. Craig, M. A. Espy, L. D. Isenhower, T. E. Kasprzyk, K. R. Knight, C. L. Morris, S. Penttila, D. Rigsby, M. E. Sadler, E. Six, H. M. Spinka, I. Supek, G. J. Wagner, and Q. Zhao, Phys. Rev. C **60**, 024604 (1999).
- [20] L. D. Isenhower, T. Black, B. M. Brooks, A. W. Brown, K. Graessle, J. A. Redmon, M. E. Sadler, J. D. Bowman, D. H. Fitzgerald, J. N. Knudson, H. W. Baer, P. Heusi, F. Irom, T. Bergman, and W. J. Briscoe, in *Proceedings of 8th International Symposium on Meson-Nucleon Physics and the Structure of the Nucleon, Zuoz, Engadine, Switzerland, Au-*

- gust 15 – 21, 1999*, edited by D. Drechsel, G. Höhler, W. Kluge, H. Leutwyler, B. M. K. Nefkens, and H.-M. Staudenmaier, π N Newsletter **15**, 292 (1999); L. D. Isenhower, private communication, 1999.
- [21] B. J. Kriss, S. Høibråten, M. D. Holcomb, M. D. Kohler, J. J. Kraushaar, S. Parry, R. A. Ristinen, A. Saunders, W. R. Smythe, C. L. Morris, M. Rawool-Sullivan, R. M. Whitton, J. T. Brack, E. F. Gibson, and J. L. Langenbrunner, Phys. Rev. C **59**, 1480 (1999); B. J. Kriss, R. A. Ristinen, S. Høibråten, M. D. Holcomb, M. D. Kohler, J. J. Kraushaar, A. Saunders, W. R. Smythe, C. L. Morris, M. Rawool-Sullivan, R. M. Whitton, J. T. Brack, E. F. Gibson, and J. L. Langenbrunner, π N Newsletter **12**, 20 (1997).
- [22] E. Frlez, D. Počanić, K. A. Assamagan, J. P. Chen, K. J. Keeter, R. M. Marshall, R. C. Minehart, L. C. Smith, G. E. Dodge, S. S. Hanna, B. H. King, and J. N. Knudson, Phys. Rev. C **57**, 3144 (1998) [hep-ex/9712024].
- [23] M. Janousch, A. Badertscher, P. F. A. Goudsmit, H. J. Leisi, E. Matsinos, P. Weber, and Z. G. Zhao, Phys. Lett. **B414**, 237 (1997).
- [24] B. A. Raue, T. A. Greco, M. G. Khayat, F. Adimi, B. van den Brandt, H. Breuer, T. Chang, N. S. Chant, H. Chen, T. A. Dooling, A. P. Dvoredsky, B. S. Flanders, T. Gu, J. P. Haas, P. Hautle, J. Huffman, J. J. Kelly, A. Klein, K. Koch, J. A. Konter, A. I. Kovalev, G. S. Kyle, J. J. Lawrie, Z. Lin, S. Mango, P. Markowitz, R. Meier, T. Payerle, S. Ritt, P. G. Roos, and M. Wang, Phys. Rev. C **53**, 1005 (1996).
- [25] Ch. Joram, M. Metzler, J. Jaki, W. Kluge, H. Matthäy, R. Wieser, B. M. Barnett, H. Clement, S. Krell, and G. J. Wagner, Phys. Rev. C **51**, 2144 (1995); Ch. Joram, M. Metzler, J. Jaki, W. Kluge, H. Matthäy, R. Wieser, B. M. Barnett, R. Bilger, H. Clement, K. Föhl, K. Heitlinger, S. Krell, and G. J. Wagner, Phys. Rev. C **51**, 2159 (1995). We used these data in our SM95 analysis [5].
- [26] R. Wieser, A. Denig, U. von Hagel, Ch. Joram, W. Kluge, R. Andermann, R. Bilger, H. Clement, K. Föhl, K. Heitlinger, G. J. Wagner, B. van den Brandt, F. Foroughi, P. Hautle, A. Konter, S. Mango, and A. Kovalev, Phys. Rev. C **54**, 1930 (1996). We used these data in our SM95 analysis [5].
- [27] I. G. Alekseev, B. M. Bobchenko, P. E. Budkovsky, V. P. Kanavets, L. I. Koroleva, V. I. Martynov, B. V. Morozov, V. M. Nesterov, V. V. Platonov, V. V. Ryltsov, V. A. Sakharov, A. D. Sulimov, D. N. Svirida, V. V. Zhurkin, V. V. Abaev, N. A. Bazhanov, V. S. Bekrenev, Yu. A. Beloglazov, E. A. Filimonov, A. I. Kovalev, N. G. Kozlenko, S. P. Kruglov, A. A. Kulbardis, I. V. Lopatin, V. A. Shchedrov, V. V. Sumachev, and V. Yu. Trautman, Phys. Lett. **B351**, 585 (1995). We used these data in our SM95 analysis [5].
- [28] I. G. Alekseev, P. E. Budkovsky, V. P. Kanavets, L. I. Koroleva, B. V. Morozov, V. M. Nesterov, V. V. Ryltsov, D. N. Svirida, A. D. Sulimov, V. V. Zhurkin, Yu. A. Beloglazov, A. I. Kovalev, S. P. Kruglov, D. V. Novinsky, V. A. Shchedrov, V. V. Sumachev, V. Yu. Trautman, N. A. Bazhanov, and E. I. Bunyatova, Phys. Lett. **B485**, 32 (2000) [hep-ex/0004025]; I. G. Alekseev, N. A. Bazhanov, Yu. A. Beloglazov, P. E. Budkovsky, E. I. Bunyatova, V. P. Kanavets, A. I. Kovalev, L. I. Koroleva, S. N. Kruglov, B. V. Morozov, V. M. Nesterov, D. V. Novinsky, V. V. Ryltsov, V. A. Shchedrov, A. D. Sulimov, V. V. Sumachev, D. N. Svirida, V. Yu. Trautman, and V. V. Zhurkin, Eur. Phys. J. A **12**, 117 (2001).
- [29] E. Pedroni, K. Gabathuler, J. J. Domingo, W. Hirt, P. Schwaller, J. Arvieux, C. H. Q. Ingram, P. Gretillat, J. Piffaretti, N. W. Tanner, and C. Wilkin, Nucl. Phys. **A300**, 321 (1978).
- [30] J. T. Brack, J. J. Kraushaar, J. H. Mitchell, R. J. Peterson, R. A. Ristinen, J. L. Ullmann, D. R. Gill, R. R. Johnson, D. Ottewell, F. M. Rozon, M. E. Sevier, G. R. Smith, F. Tervisidis, R. P. Trelle, and E. L. Mathie, Phys. Rev. C **34**, 1771 (1986).
- [31] A. A. Carter, J. R. Williams, D. V. Bugg, P. J. Bussey, and D. R. Dance, Nucl. Phys. **B26**, 445 (1971).
- [32] P. J. Bussey, J. R. Carter, D. R. Dance, D. V. Bugg, A. A. Carter, and A. M. Smith, Nucl. Phys. **B58**, 363 (1973).
- [33] The uncertainties on Refs. [31, 32] were updated to take into account beam-energy uncertainty effects. Correspondence to R. A. Arndt from D. V. Bugg. A slightly different treatment of of this data is chosen in Ref. [57].
- [34] T. W. Morrison, Ph. D. Thesis, The George Washington University, Dec. 1999 (unpublished).
- [35] D. M. Binnie, L. Camilleri, N. C. Debenham, A. Duane, D. A. Garbutt, J. R. Holmes, W. G. Jones, J. Keyne, M. Lewis, I. Siotis, P. N. Upadhyay, I. F. Burton, and J. G. McEwen, Phys. Rev. D **8**, 2789 (1973).
- [36] F. Bulos, R. E. Lanou, A. E. Pifer, A. M. Shapiro, C. A. Bordner, A. E. Brenner, M. E. Law, E. E. Ronat, F. D. Rudnick, K. Strauch, J. J. Szymanski, P. Bastien, B. B. Brabson, Y. Eisenberg, B. T. Feld, V. K. Kistiakowsky, I. A. Pless, L. Rosenson, R. K. Yamamoto, G. Calvelli, F. Gasparini, L. Guerriero, G. A. Slakndin, A. Tomasin, L. Ventura, C. Voci, and F. Waldner, Phys. Rev. **187**, 1827 (1969).
- [37] N. C. Debenham, D. M. Binnie, L. Camilleri, J. Carr, A. Duane, D. A. Garbutt, W. G. Jones, J. Keyne, I. Siotis, and J. G. McEwen, Phys. Rev. D **12**, 2545 (1975).
- [38] W. Deinet, H. Mueller, D. Schmitt, H. M. Staudenmaier, S. Buniatov, and E. Zavattini, Nucl. Phys. **B11**, 495 (1969).
- [39] W. B. Richards, C. B. Chiu, R. D. Eandi, A. C. Helmholz, R. W. Kenney, B. J. Moyer, J. A. Poirier, R. J. Cence, V. Z. Peterson, N. K. Sehgal, and V. J. Stenger, Phys. Rev. D **1**, 10 (1970).
- [40] R. M. Brown, A. G. Clark, P. J. Duke, W. M. Evans, R. J. Gray, E. S. Groves, R. J. Ott, H. R. Renshall, T. P. Shah, A. J. Shave, J. J. Thresher, and M. W. Tyrrell, Nucl. Phys. **B153**, 89 (1979).
- [41] J. Feltesse, R. Ayed, P. Bareyre, P. Borgeaud, M. David, J. Ernwein, Y. Lemoigne, and G. Villet, Nucl. Phys. **B93**, 242 (1975).
- [42] V. Z. Peterson *et al.*, Dubna Preprint, 30-64 (1964) (unpublished); A. Baldini, V. Flaminio, W. G. Moorhead, and D. R. O. Morrison, *Total Cross-Sections for Reactions of High Energy Particles*, Landolt-Börnstein Vol. **I/12a**, edited

- by H. Schopper (Springer Verlag, 1988).
- [43] M. Basile, D. Bollini, P. Dalpiaz, P. L. Frabetti, T. Massam, F. Navach, F. L. Navarra, M. Schneegans, and A. Zichichi, *Nuovo Cim.* **A3**, 371 (1971).
- [44] R. T. Van de Walle, C. L. A. Pols, D. J. Schotanus, H. J. G. M. Tiecke, and D. Z. Toet, *Nuovo Cim.* **A53**, 745 (1968).
- [45] R. B. Chaffee, Ph. D. Thesis, Lawrence Berkeley Laboratory, LBL-1060, 1975 (unpublished).
- [46] J. E. Nelson, Ph. D. Thesis, Lawrence Berkeley Laboratory, LBL-1019, 1972 (unpublished).
- [47] M. Clajus and B. M. K. Nefkens, *πN Newsletter* **7**, 76 (1992).
- [48] A. Baldini, V. Flaminio, W. G. Moorhead, and D. R. O. Morrison, *Total Cross-Sections for Reactions of High Energy Particles*, Landolt-Börnstein Vol. **I/12a**, edited by H. Schopper (Springer Verlag, 1988).
- [49] We thank G. Höhler for emphasizing this point.
- [50] G. F. Chew and F. E. Low, *Phys. Rev.* **101**, 1570 (1956).
- [51] J. Hamilton, “Pion-Nucleon Interactions,” in *High Energy Physics*, edited by E. H. S. Burhop (Academic Press, New York, 1964), p. 193.
- [52] In what follows, \pm subscripts denote charge channels, superscripts denote isospin channels, s , t , and u are the usual Mandelstam variables, and M is the nucleon mass.
- [53] J. Gasser, H. Leutwyler, M. P. Locher, and M. E. Sainio, *Phys. Lett.* **B213**, 85 (1988); *ibid.* **B253**, 252 (1991); *ibid.* **B253**, 260 (1991).
- [54] R. Koch, *Z. Phys. C* **29**, 597 (1985).
- [55] H.-C. Schröder, A. Badertscher, P. F. A. Goudsmit, M. Janousch, H. J. Leisi, E. Matsinos, D. Sigg, Z. G. Zhao, D. Chatellard, J.-P. Egger, E. Jeannet, K. Gabathuler, P. Hauser, L. M. Simons, and A. J. R. El Hassani, *Phys. Lett.* **B469**, 25 (1999).
- [56] J. Gasser, A. Rusetsky, and I. Scimemi, Eprint hep-ph/0305260.
- [57] D. V. Bugg and M. D. Scadron, to be published in *Eur. J. Phys. C* [hep-ph/0312346]. Our mass and width difference is most consistent with Fit 1 of this study.
- [58] B. Tromborg, S. Waldenstrom, and I. Overbo, *Phys. Rev. D* **15**, 725 (1977); *Helv. Phys. Acta* **51**, 584 (1978).
- [59] R. Koch and E. Pietarinen, *Nucl. Phys.* **A336**, 331 (1980).
- [60] W. R. Gibbs, private communication. The charge distribution was assumed exponential with an r.m.s. radius of 0.86 fm.
- [61] D. V. Bugg, *Nucl. Phys.* **B58**, 397 (1973); we thank D. V. Bugg for pointing out this correction.
- [62] We thank D. M. Manley and G. Höhler for comments leading to the discovery of this error.
- [63] G. A. Miller, B. M. K. Nefkens, and I. Slaus, *Phys. Rep.* **194**, 1 (1990).
- [64] S. Weinberg, in *Chiral Dynamics: Theory and Experiment*, edited by A. M. Bernstein and B. R. Holstein (Springer Verlag, 1994) p. 3.
- [65] U.-G. Meissner, in *Proceedings of 9th International Symposium on Meson-Nucleon Physics and the Structure of the Nucleon (MENU2001), Washington, DC, USA, July 26 – 31, 2001*, edited by H. Haberzettl and W. J. Briscoe, *πN Newsletter* **16**, 1 (2002) [hep-ph/0108133].
- [66] W. R. Gibbs, L. Ai, and W. B. Kaufmann, *Phys. Rev. Lett.* **74**, 3740 (1995).
- [67] A. Gashi, E. Matsinos, G. C. Oades, G. Rasche, and W. S. Woolcock, Eprint nucl-th/0009081, submitted to *Nucl. Phys. A*.
- [68] N. Fettes and Ulf-G. Meissner, *Phys. Rev. C* **63**, 045201 (2001) [Eprint hep-ph/0008181].
- [69] N. Fettes and Ulf-G. Meissner, *Nucl. Phys.* **A693** 693 (2001) [Eprint hep-ph/0101030].
- [70] J. F. Martin, J. C. Sleeman, R. M. Brown, P. J. Duke, W. M. Evans, E. S. Groves, R. E. Hill, W. R. Holley, D. P. Jones, J. J. Thresher, and M. W. Tyrrell, *Nucl. Phys.* **B89**, 253 (1975).
- [71] Y. Suzuki, T. Adachi, M. Daigo, Y. Hemmi, R. Kikuchi, M. Minowa, K. Miyake, S. Naito, T. Nakamura, M. Sakuda, I. Nakano, and M. Kobayashi, *Nucl. Phys.* **B294**, 961 (1987).
- [72] V. V. Baru, A. E. Kudryavtsev, V. E. Tarasov, W. J. Briscoe, K. S. Dhuga, and I. I. Strakovsky, *Phys. Rev. C* **62**, 044003 (2000) [Eprint nucl-th/9910011];
A. E. Kudryavtsev, V. E. Tarasov, W. J. Briscoe, B. L. Berman, K. S. Dhuga, and I. I. Strakovsky, *Phys. Rev. C* **66**, 0540007 (2002) [Eprint nucl-th/0109074].
- [73] D.V. Bugg, A.A. Carter, and J.R. Carter, *Phys. Lett.* **44B**, 278 (1973).
- [74] H.-Ch. Schröder, A. Badertscher, P. F. A. Goudsmith, M. Janousch, J. J. Leisi, E. Matsinos, D. Sigg, Z. G. Zhao, D. Chatellard, J.-P. Egger, K. Gabathuler, P. Hauser, L. M. Simons, and A. J. Rusi El Hassani, *Eur. Phys. J. C* **21**, 473 (2001).
- [75] J. J. de Swart, M. C. M. Rentmeester, and R. G. E. Timmermans, in *Proceedings of 7th International Symposium on Meson-Nucleon Physics and the Structure of the Nucleon, Vancouver, BC, Canada, July 28–Aug. 1, 1997*, edited by D. Drechsel, G. Höhler, W. Kluge, H. Leutwyler *et al.* *πN Newslett.* **13**, 96 (1997) [Eprint nucl-th/9802084].
- [76] T. E. O. Ericson, B. Loiseau, and S. Wycech, Eprint hep-ph/0310134.
- [77] D. F. Anagnostopoulos, H. Fuhrmann, D. Gotta, A. Gruber, M. Hennebach, P. Indelicato, Y.-W. Liu, B. Manil, V. M. Markushin, N. Nelms, L. M. Simons, and J. Zmeskal in *Proceedings of 9th International Symposium on Meson-Nucleon Physics and the Structure of the Nucleon (MENU2001), Washington, DC, USA, July 26–31, 2001*, edited by H. Haberzettl and W. J. Briscoe, *πN Newslett.* **16**, 355 (2002).
- [78] J.-R. Argand, *Essai sur une maniere de représenter les quantités imaginaires dans les constructions géométriques*, (Sans

nom d'auteur). (Paris, 1806) I vol. petit in-8°, 78 pages.

TABLE I: Comparison of present (FA02) and previous (SM95 [5], FA93 [8], SM90 [9], and FA84 [4]) energy-dependent partial-wave analyses of elastic $\pi^\pm p$, charge-exchange ($\pi^0 n$), and $\pi^- p \rightarrow \eta n$ (ηn) scattering data. For FA02 solution, ηN data has been included to 800 MeV. The χ^2 values for the previous solutions correspond to our published results. N_{prm} is the number of parameters ($I = 1/2$ and $3/2$) varied in the fit.

Solution	Range (MeV)	χ^2/π^+p	χ^2/π^-p	χ^2/π^0n	$\chi^2/\eta n$	N_{prm}
FA02	2100	21735/10468	18932/9650	4136/1690	439/173	94/78
SM95	2100	23593/10197	18855/9421	4442/1625	–	94/80
FA93	2100	23552/10106	20747/9304	4834/1668	–	83/77
SM90	2100	24897/10031	24293/9344	10814/2132	–	76/68
FA84	1100	7416/ 3771	10658/4942	2062/ 717	–	64/57

TABLE II: Comparison of χ^2/data for normalized (Norm) and unnormalized (Unnorm) data used in the FA02 solution.

Reaction	Norm	Unnorm
$\pi^+p \rightarrow \pi^+p$	2.1	9.3
$\pi^-p \rightarrow \pi^-p$	2.0	7.1
$\pi^-p \rightarrow \pi^0n$	2.4	9.5
$\pi^0n \rightarrow \eta n$	2.5	4.6

TABLE III: Single-energy (binned) fits of combined elastic $\pi^\pm p$, charge-exchange, $\pi^- p \rightarrow \eta n$ scattering data, and χ^2 values. N_{prm} is the number of parameters varied in the single-energy fits, and χ_E^2 is given by the energy-dependent fit, FA02, over the same energy interval.

T_π (MeV)	Range (MeV)	N_{prm}	χ^2/data	χ_E^2	T_π (MeV)	Range (MeV)	N_{prm}	χ^2/data	χ_E^2
30	26 – 33	4	171/141	218	795	793 – 796	30	204/165	301
47	45 – 49	4	74/ 82	80	820	813 – 827	30	399/302	436
66	61 – 69	4	183/136	198	868	864 – 870	31	294/211	389
90	87 – 92	4	116/111	154	888	886 – 890	32	174/144	291
112	107 – 117	6	114/ 93	115	902	899 – 905	34	539/416	891
124	121 – 126	6	84/ 60	92	927	923 – 930	34	234/200	378
142	139 – 146	6	230/159	213	962	953 – 971	34	387/299	593
170	165 – 174	6	177/141	170	1000	989 –1015	36	691/423	847
193	191 – 195	6	103/107	119	1030	1022 –1039	38	286/272	396
217	214 – 220	6	116/109	143	1044	1039 –1048	38	362/243	520
238	235 – 241	6	124/115	149	1076	1073 –1078	38	240/218	432
266	263 – 271	6	162/123	175	1102	1099 –1103	39	232/173	346
292	291 – 293	8	157/129	199	1149	1147 –1150	40	339/210	468
309	306 – 310	8	160/140	174	1178	1165 –1192	41	759/394	925
334	332 – 335	8	94/ 58	130	1210	1203 –1216	42	286/233	364
352	351 – 352	9	82/110	99	1243	1237 –1248	44	473/283	586
389	387 – 390	10	31/ 28	74	1321	1304 –1337	44	731/401	946
425	424 – 425	10	151/139	191	1373	1371 –1374	46	331/166	613
465	462 – 467	13	358/120	451	1403	1389 –1417	48	544/408	811
500	499 – 501	16	161/136	209	1458	1455 –1460	48	279/258	504
518	515 – 520	18	104/ 78	144	1476	1466 –1486	48	510/344	682
534	531 – 535	18	131/128	184	1570	1554 –1586	48	834/546	1062
560	557 – 561	19	310/151	582	1591	1575 –1606	48	402/336	588
580	572 – 590	20	382/286	556	1660	1645 –1673	48	510/391	732
599	597 – 600	22	253/151	382	1720	1705 –1734	48	388/279	510
625	622 – 628	24	125/ 94	204	1753	1739 –1766	48	654/439	864
662	648 – 675	25	554/352	735	1838	1829 –1845	48	444/290	698
721	717 – 725	28	160/129	217	1875	1852 –1897	48	948/674	1284
745	743 – 746	28	159/100	286	1929	1914 –1942	48	857/501	1187
765	762 – 767	30	190/167	289	1970	1962 –1978	48	461/271	684
776	774 – 778	30	220/155	302	2026	2014 –2037	48	368/320	652

TABLE IV: Resonance couplings from a Breit-Wigner fit to the FA02 solution [GW], our previous solution SM95 [VPI] [5], and an average from the Review of Particle Properties [RPP] [1] (in square brackets). Masses W_R , half-widths $\Gamma/2$, and partial widths for $\Gamma_{\pi N}/\Gamma$ are listed for isospin 1/2 baryon resonances N^* .

Resonance	W_R (MeV)	$\Gamma/2$ (MeV)	$\Gamma_{\pi N}/\Gamma$	Ref
$P_{11}(1440)$	1468.0 ± 4.5	180 ± 13	0.750 ± 0.024	GW
	1467	220	0.68	VPI
	[1440]	[175]	[0.65]	RPP
$D_{13}(1520)$	1516.3 ± 0.8	49.3 ± 1.3	0.640 ± 0.005	GW
	1515	53	0.61	VPI
	[1520]	[60]	[0.55]	RPP
$S_{11}(1535)$	1546.7 ± 2.2	89.0 ± 5.8	0.360 ± 0.009	GW
	1535	33	0.31	VPI
	[1535]	[75]	[0.45]	RPP
$S_{11}(1650)$	1651.2 ± 4.7	65.3 ± 3.5	1.000	GW
	1667	45	≈ 1.0	VPI
	[1650]	[75]	[0.72]	RPP
$D_{15}(1675)$	1676.2 ± 0.6	75.9 ± 1.5	0.400 ± 0.002	GW
	1673	77	0.38	VPI
	[1675]	[75]	[0.45]	RPP
$F_{15}(1680)$	1683.2 ± 0.7	67.2 ± 1.9	0.670 ± 0.004	GW
	1678	63	0.68	VPI
	[1680]	[65]	[0.65]	RPP
$P_{13}(1720)$	1749.6 ± 4.5	128 ± 11	0.190 ± 0.004	GW
	1820	177	0.16	VPI
	[1720]	[75]	[0.15]	RPP
$G_{17}(2190)$	2192.1 ± 8.7	363 ± 31	0.230 ± 0.002	GW
	2131	238	0.23	VPI
	[2190]	[225]	[0.15]	RPP
$H_{19}(2220)$	2270 ± 11	183 ± 21	0.200 ± 0.006	GW
	2258	167	0.26	VPI
	[2220]	[200]	[0.15]	RPP
$G_{19}(2250)$	2376 ± 43	462 ± 89	0.110 ± 0.004	GW
	2291	386	0.10	VPI
	[2250]	[200]	[0.10]	RPP

TABLE V: Parameters for isospin 3/2 baryon resonances Δ^* . Notation as in Table IV.

Resonance	W_R (MeV)	$\Gamma/2$ (MeV)	$\Gamma_{\pi N}/\Gamma$	Ref
$P_{33}(1232)$	1232.9 ± 1.2	59.0 ± 1.1	1.000	GW
	1233	57	≈ 1.0	VPI
	[1232]	[60]	[>0.99]	RPP
$S_{31}(1620)$	1614.1 ± 1.1	70.5 ± 3.0	0.310 ± 0.004	GW
	1617	54	0.29	VPI
	[1620]	[75]	[0.25]	RPP
$D_{33}(1700)$	1687.9 ± 2.5	182.4 ± 8.3	0.150 ± 0.001	GW
	1680	136	0.16	VPI
	[1700]	[150]	[0.15]	RPP
$F_{35}(1905)$	1855.7 ± 4.2	167 ± 11	0.120 ± 0.002	GW
	1850	147	0.12	VPI
	[1905]	[175]	[0.10]	RPP
$D_{35}(1930)$	2046 ± 45	201 ± 99	0.040 ± 0.014	GW
	2056	295	0.11	VPI
	[1930]	[175]	[0.15]	RPP
$F_{37}(1950)$	1923.3 ± 0.5	139.1 ± 1.5	0.480 ± 0.002	GW
	1921	116	0.49	VPI
	[1950]	[150]	[0.37]	RPP

TABLE VI: Pole positions from the solution FA02 [GW], our previous solution SM95 [VPI] [5], and an average from the Particle Data Group [RPP] [1] (in square brackets). $Re(W_R)$ and $Im(W_I)$ parts are listed for isospin 1/2 baryon resonances. Second sheet poles are labeled by †. Modulus and phase values are listed for the πN elastic pole residue.

Wave	W_R	$-W_I$	Modulus	Phase	Ref	Wave	W_R	$-W_I$	Modulus	Phase	Ref
	(MeV)	(MeV)	(MeV)	(deg)			(MeV)	(MeV)	(MeV)	(deg)	
S_{11}	1526	65	33	14	GW	D_{15}	1659	73	29	-22	GW
	1501	62	31	-12	VPI		1663	76	29	-6	VPI
	[1505]	[85]	-	-	RPP		[1660]	[70]	-	-	RPP
S_{11}	1653	91	69	-55	GW	F_{15}	1678	60	43	1	GW
	1673	41	22	29	VPI		1670	60	40	1	VPI
	[1660]	[80]	-	-	RPP		[1670]	[60]	-	-	RPP
P_{11}	1357	80	36	-102	GW	F_{15}	1779	124	47	-61	GW
	1346	88	42	-101	VPI		1793	94	27	-56	VPI
	[1365]	[105]	-	-	RPP		-	-	-	-	RPP
P_{11}^\dagger	1385	83	82	-51	GW	G_{17}	2076	251	68	-32	GW
	1383	105	92	-54	VPI		2030	230	46	-23	VPI
	-	-	-	-	RPP		[2050]	[225]	-	-	RPP
P_{13}	1655	139	20	-88	GW	G_{19}	2238	268	33	-25	GW
	1717	194	39	-70	VPI		2087	340	24	-44	VPI
	[1700]	[125]	-	-	RPP		[2140]	[240]	-	-	RPP
D_{13}	1514	51	35	-6	GW	H_{19}	2209	282	96	-71	GW
	1515	55	34	7	VPI		2203	268	68	-43	VPI
	[1510]	[57]	-	-	RPP		[2170]	[235]	-	-	RPP

TABLE VII: Pole positions for isospin 3/2 baryon resonances Δ^* . Notation as in Table VI.

Wave	W_R (MeV)	$-W_I$ (MeV)	Modulus (MeV)	Phase (deg)	Ref
S_{31}	1594	59	17	-104	GW
	1585	52	14	-121	VPI
	[1600]	[57]	-	-	RPP
P_{31}	1748	262	48	158	GW
	1810	247	53	-176	VPI
	[1855]	[175]	-	-	RPP
P_{33}	1210	50	53	-47	GW
	1211	50	38	-22	VPI
	[1210]	[50]	-	-	RPP
D_{33}	1617	113	16	-47	GW
	1655	121	16	-12	VPI
	[1660]	[100]	-	-	RPP
D_{35}	1966	182	16	-21	GW
	1913	123	8	-47	VPI
	[1890]	[125]	-	-	RPP
F_{35}	1825	135	16	-25	GW
	1832	127	12	-4	VPI
	[1830]	[140]	-	-	RPP
F_{37}	1874	118	57	-34	GW
	1880	118	54	-17	VPI
	[1885]	[120]	-	-	RPP

TABLE VIII: Zero positions from the solution FA02 [GW] and our previous solution SM95 [VPI] [5]. $Re(W_R)$ and $Im(W_I)$ parts are listed for isospin 1/2 and 3/2 baryon resonances.

Wave	W_R (MeV)	$-W_I$ (MeV)	Ref
S_{11}	1578	38	GW
	1582	54	VPI
	1695	43	VPI
P_{13}	1585	51	GW
	1618	85	VPI
D_{13}	1759	64	GW
	1751	87	VPI
F_{15}	1765	66	GW
	1775	57	VPI
S_{31}	1580	36	GW
	1579	30	VPI
P_{31}	1826	197	GW
	1863	170	VPI
D_{35}	1806	107	GW
	1827	69	VPI

TABLE IX: Comparison of FA02 and Breit-Wigner+background fits. Background parameters for isospin 1/2 baryon resonance fits (see text and associated Table IV). “Data” refers to the number of scattering data used in the fit.

Resonance	Wmin (MeV)	Wmax (MeV)	BW fit χ^2	FA02 χ^2	Data	A	B	C
$P_{11}(1440)$	1350	1550	5556	5587	2393	-0.270±0.026	–	–
$D_{13}(1520)$	1480	1560	3238	3341	1448	-0.035±0.013	–	–
$S_{11}(1535)$	1490	1590	3566	3657	1632	0.342±0.018	4.530±0.851	–
$S_{11}(1650)$	1600	1720	6992	7218	3394	-0.584±0.073	2.415±1.356	0.414±0.024
$D_{15}(1675)$	1610	1730	7343	7359	3546	-0.034±0.004	–	–
$F_{15}(1680)$	1620	1730	6683	6650	3172	0.011±0.011	1.192±0.575	–
$P_{13}(1720)$	1650	1790	8321	8484	4160	-0.127±0.008	1.463±0.239	–
$G_{17}(2190)$	2049	2249	8017	8040	3774	0.024±0.009	–	–
$H_{19}(2220)$	2140	2250	5675	5682	2554	0.028±0.010	–	–
$G_{19}(2250)$	2010	2258	11020	11025	5330	-0.046±0.010	–	–

TABLE X: Comparison of FA02 and Breit-Wigner+background fits. Background parameters for isospin 3/2 baryon resonance fits (see text and associated Table V). “Data” refers to the number of scattering data used in the fit.

Resonance	Wmin (MeV)	Wmax (MeV)	BW fit χ^2	FA02 χ^2	Data	A
$P_{33}(1232)$	1180	1270	1180	1185	920	0.035±0.017
$S_{31}(1620)$	1570	1680	5187	5212	2321	-0.851±0.013
$D_{33}(1700)$	1610	1770	9624	9690	4725	-0.145±0.003
$F_{35}(1905)$	1770	1920	8069	8096	3791	-0.092±0.004
$D_{35}(1930)$	1870	2100	9912	9881	5059	-0.063±0.014
$F_{37}(1950)$	1800	2000	10623	10552	4951	0.024±0.006

TABLE XI: Parameters for low-lying resonances of isospin 1/2 and 3/2 in a fit unconstrained by dispersion relations.

Resonance	W_R (MeV)	$\Gamma/2$ (MeV)	$\Gamma_{\pi N}/\Gamma$
$P_{11}(1440)$	1473.0	200.9	0.695
$D_{13}(1520)$	1516.2	50.8	0.655
$S_{11}(1535)$	1545.4	87.0	0.385
$S_{11}(1650)$	1658.9	55.3	1.000
$D_{15}(1675)$	1673.7	75.9	0.396
$F_{15}(1680)$	1677.8	64.1	0.692
$P_{13}(1720)$	1807.1	239	0.195
$P_{33}(1232)$	1233.3	59.3	1.000
$S_{31}(1620)$	1614.0	70.1	0.316
$D_{33}(1700)$	1684.9	168.6	0.151
$F_{35}(1905)$	1861.3	159	0.119

TABLE XII: Comparison of χ^2 for the FA02 (full data set) and X370 (no charge-exchange data) solutions to 2.1 GeV ($\pi^- p \rightarrow \eta n$ data to 800 MeV). Results to 500 MeV have been listed in brackets, where one observes little or no difference in the fit quality between FA02 and X370, even for the charge-exchange database. “Data” refers to the number of scattering data used in the fit.

Reaction	Observable	FA02	X370	Data
$\pi^+ p \rightarrow \pi^+ p$	$d\sigma/d\Omega$	14574 (2043)	14624 (2033)	7246 (977)
	σ_{tot}	257 (115)	220 (115)	105 (60)
	P	6801 (533)	6629 (536)	3012 (495)
	R	28 (20)	29 (20)	48 (26)
	A	39 (24)	42 (25)	48 (26)
$\pi^- p \rightarrow \pi^- p$	$d\sigma/d\Omega$	13799 (1443)	13760 (1453)	7331 (773)
	σ_{tot}	531 (111)	445 (110)	151 (59)
	P	4441 (562)	4501 (564)	2045 (337)
	R	107 (24)	104 (23)	61 (27)
	A	49 (14)	47 (14)	60 (26)
$\pi^- p \rightarrow \pi^0 n$	$d\sigma/d\Omega$	3180 (697)	5093 (739)	1333 (379)
	σ_{tot}	24 (23)	24 (23)	34 (33)
	P	933 (194)	1175 (215)	323 (159)
$\pi^- p \rightarrow \eta n$	$d\sigma/d\Omega$	373	376	138
	σ_{tot}	67	75	35

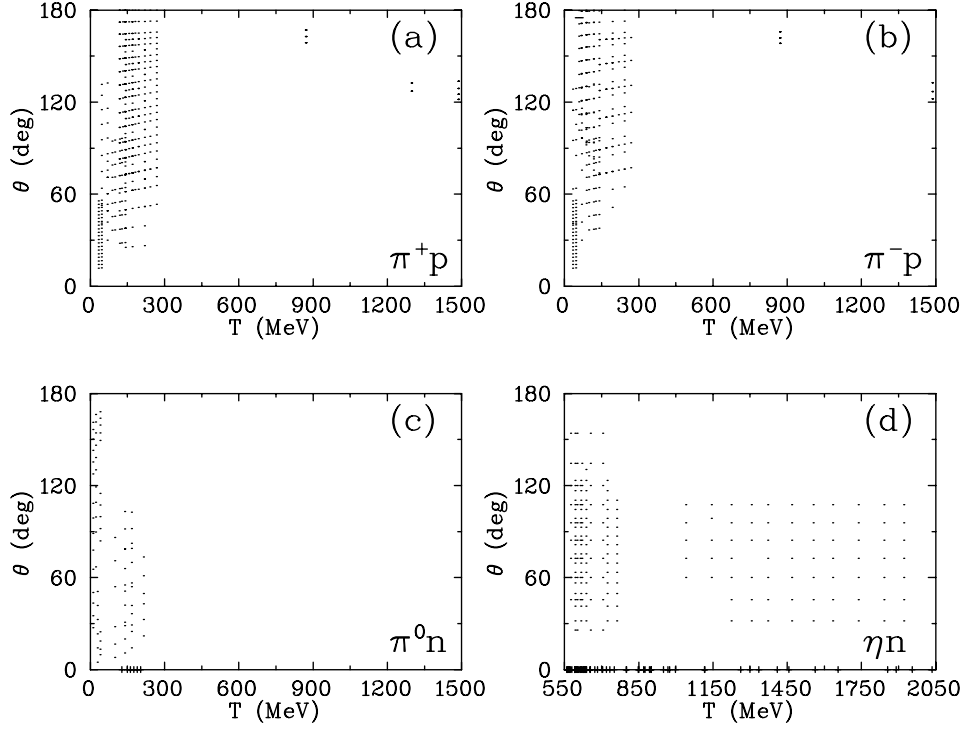


FIG. 1: Energy-angle distribution of recent (post-1995) data: (a) π^+p and (b) π^-p elastic scattering, (c) charge-exchange $\pi^-p \rightarrow \pi^0n$, and $\pi^-p \rightarrow \eta n$ (all available). Total cross sections are plotted at zero degrees.

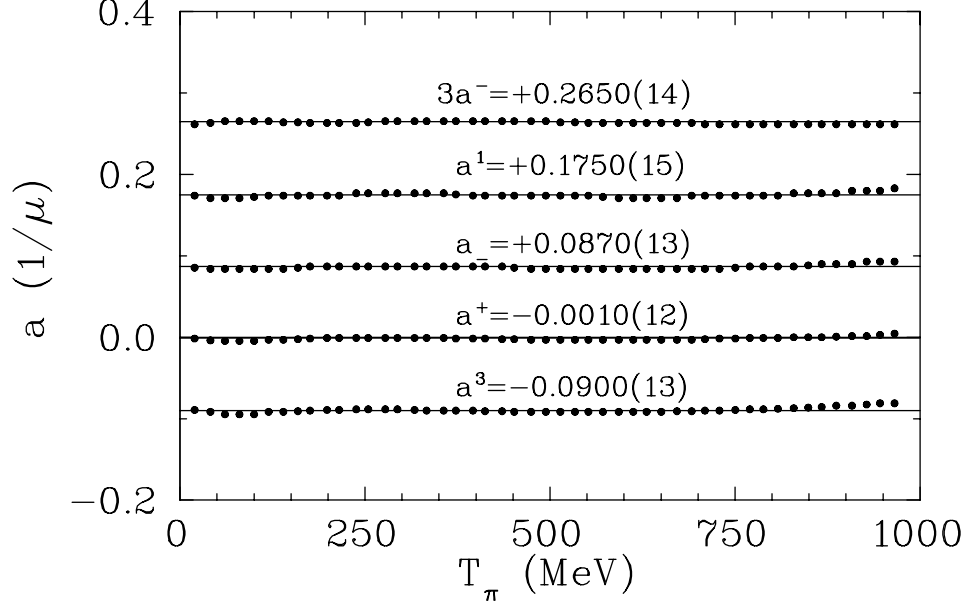


FIG. 2: Subtraction constants as a function of pion kinetic energy for the forward C^\pm dispersion relations plotted in terms of the S-wave scattering lengths a^\pm , and other combinations, in inverse pion mass units. Horizontal lines represent the least-square averages of individual values.

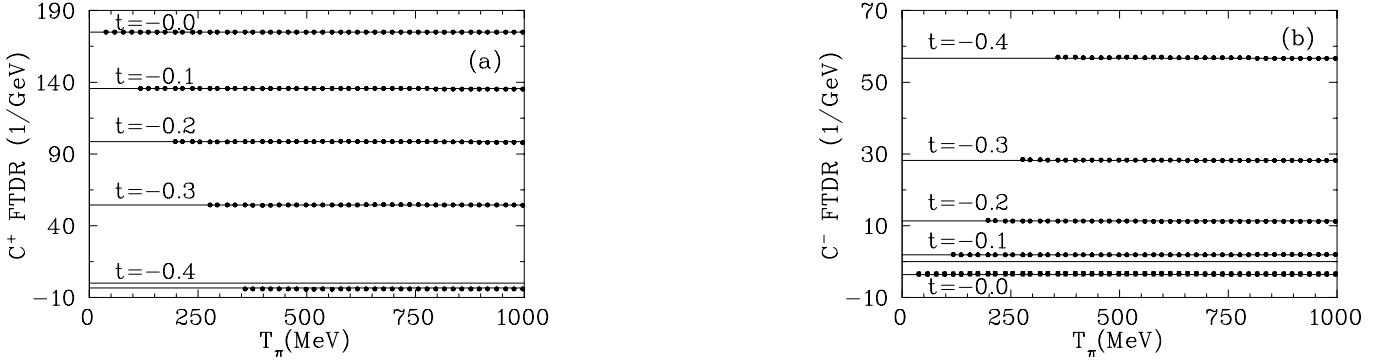


FIG. 3: Subtraction constants as a function of pion kinetic energy at four values of four-momentum transfer t [in $(GeV/c)^2$] for the fixed- t (a) $C^+(\nu, t)$ and (b) $C^-(\nu, t)$ dispersion relations. Horizontal lines represent the least-square averages of individual values.

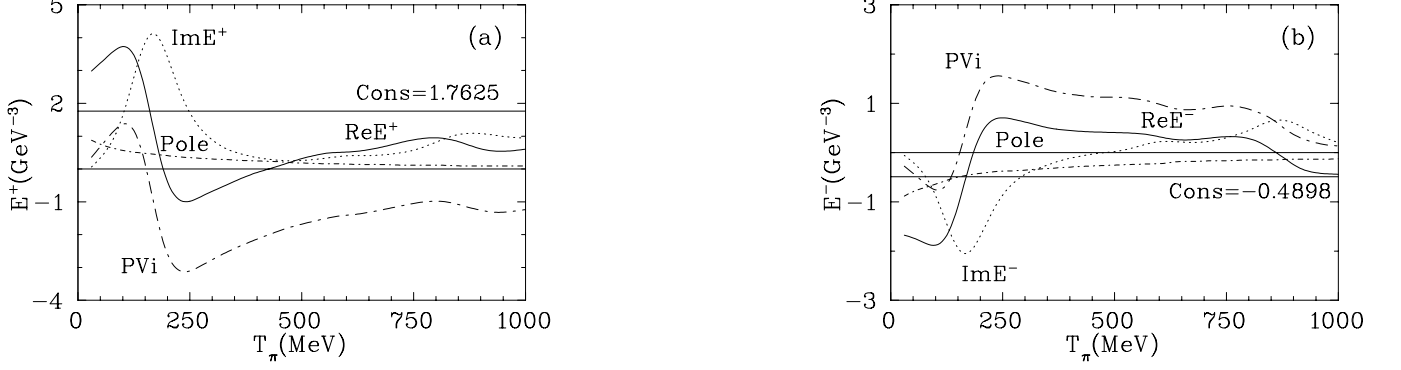


FIG. 4: Forward derivative (a) $E^+(\omega)$ and (b) $E^-(\omega)$ dispersion relations. ReE (ImE) are plotted by solid (dashed) lines, the principal value integral, PVi, by dash-dotted lines, and the pole term by short-dash-dotted lines. The respective subtraction constants are shown as horizontal solid lines.

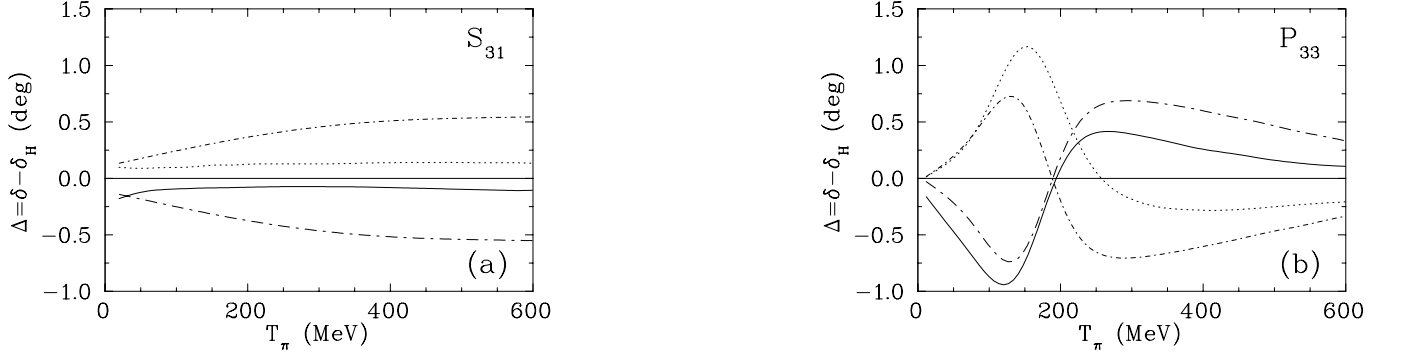


FIG. 5: Comparison of the point-Coulomb (SM95) and Nordita-Gibbs (FA02) charge corrections $\Delta = \delta - \delta_H$, the subscript H denoting an hadronic phase, for the (a) S_{31} and (b) P_{33} partial waves. In both plots, dash-dotted and short-dash-dotted (solid and dotted) curves give point-Coulomb [5] (FA02) corrections for π^+p and π^-p , respectively.

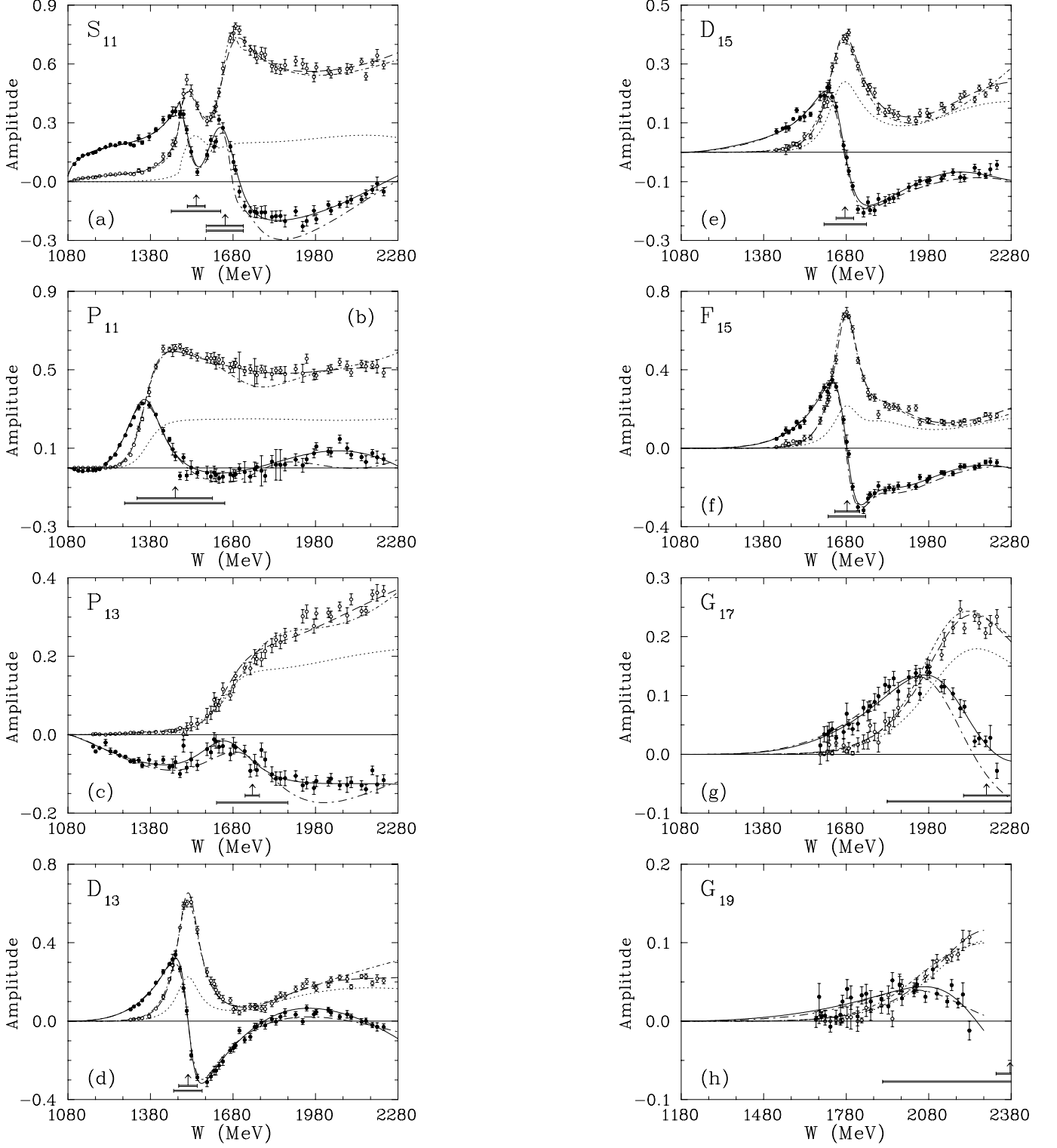


FIG. 6: Isospin 1/2 partial-wave amplitudes ($L_{2I,2J}$) from $T_\pi = 0$ to 2.1 GeV. Solid (dashed) curves give the real (imaginary) parts of amplitudes corresponding to the FA02 solution. The real (imaginary) parts of single-energy solutions are plotted as filled (open) circles. The previous SM95 solution [5] is plotted with long dash-dotted (real part) and short dash-dotted (imaginary part) lines. The dotted curve gives the unitarity limit ($ImT - T^*T$) from FA02. All amplitudes are dimensionless. Vertical arrows indicate W_R and horizontal bars show full $\Gamma/2$ and partial widths for $\Gamma_{\pi N}$ associated with the FA02 results presented in Table IV. (a) S_{11} , (b) P_{11} , (c) P_{13} , (d) D_{13} , (e) D_{15} , (f) F_{15} , (g) G_{17} , and (h) G_{19} .

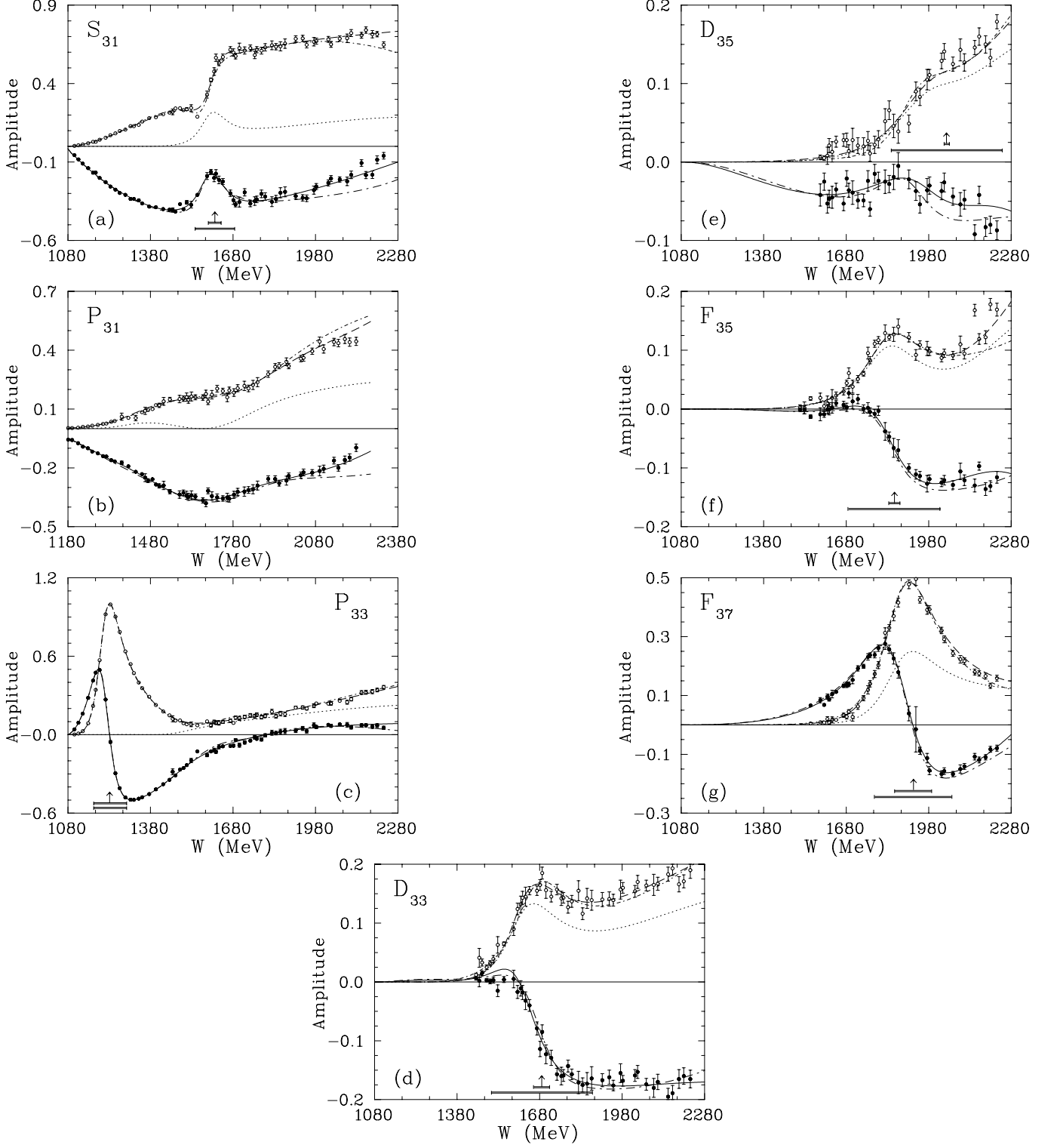


FIG. 7: Isospin 3/2 partial-wave amplitudes ($L_{2I,2J}$) from $T_\pi = 0$ to 2.1 GeV. Notation as in Fig. 6. Vertical arrows indicate W_R and horizontal bars show full $\Gamma/2$ and partial widths for $\Gamma_{\pi N}$ associated with the FA02 results presented in Table V. (a) S_{31} , (b) P_{31} , (c) P_{33} , (d) D_{33} , (e) D_{35} , (f) F_{35} , and (g) F_{37} .

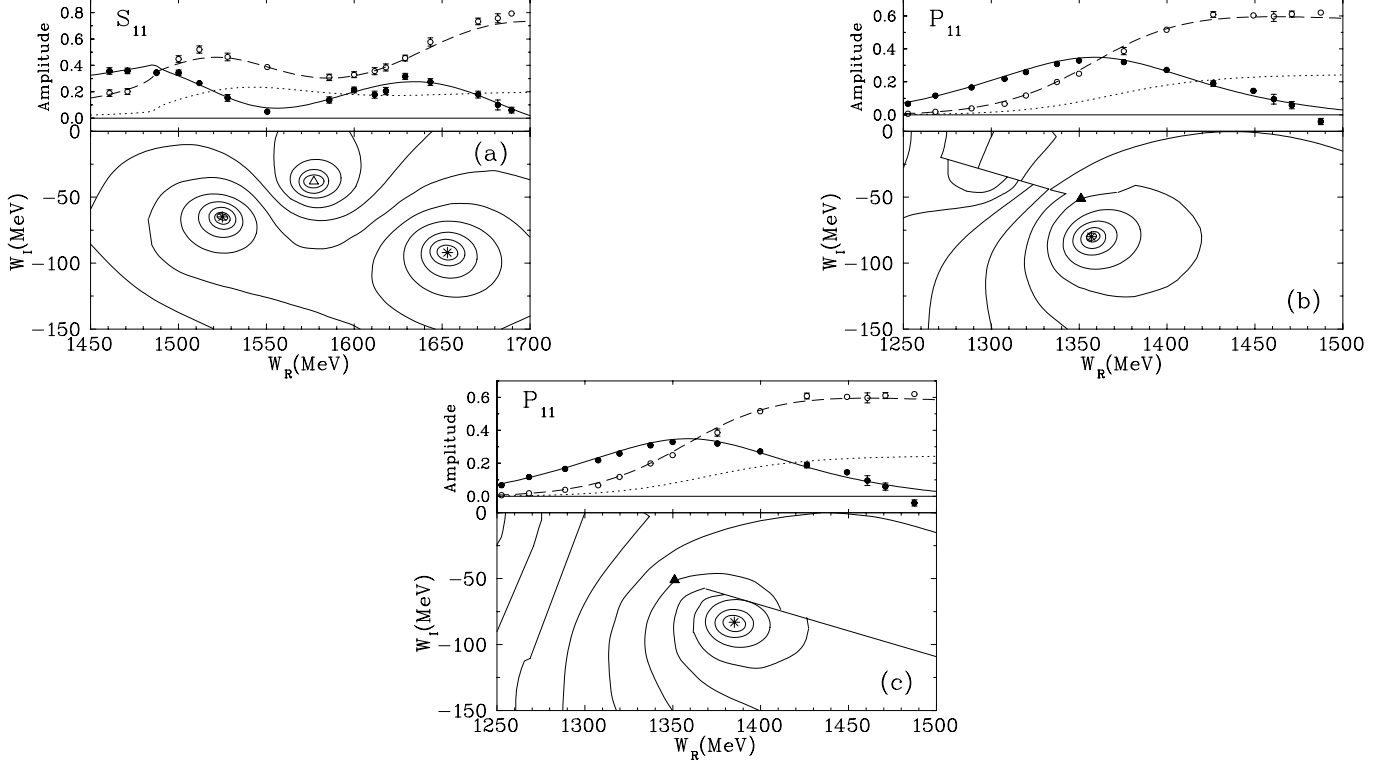


FIG. 8: Contour plot of $\ln|T|^2$ displaying complex plane structures. (a) S_{11} . Poles: $W_P = 1526 - i65$ MeV and $W_P = 1653 - i91$ MeV, shown as stars. Zero: $W_Z = 1578 - i38$ MeV, represented as an open triangle; (b) P_{11} , first sheet. Pole: $W_P = 1357 - i80$ MeV, shown as a star; and (c) P_{11} , second sheet. Pole: $W_P = 1385 - i83$ MeV, shown as a star. The branch point for P_{11} , $1349 - i50$ MeV, is represented as a solid triangle. The $\pi\Delta$ branching cut in (b) and (c) is shown as a solid line.

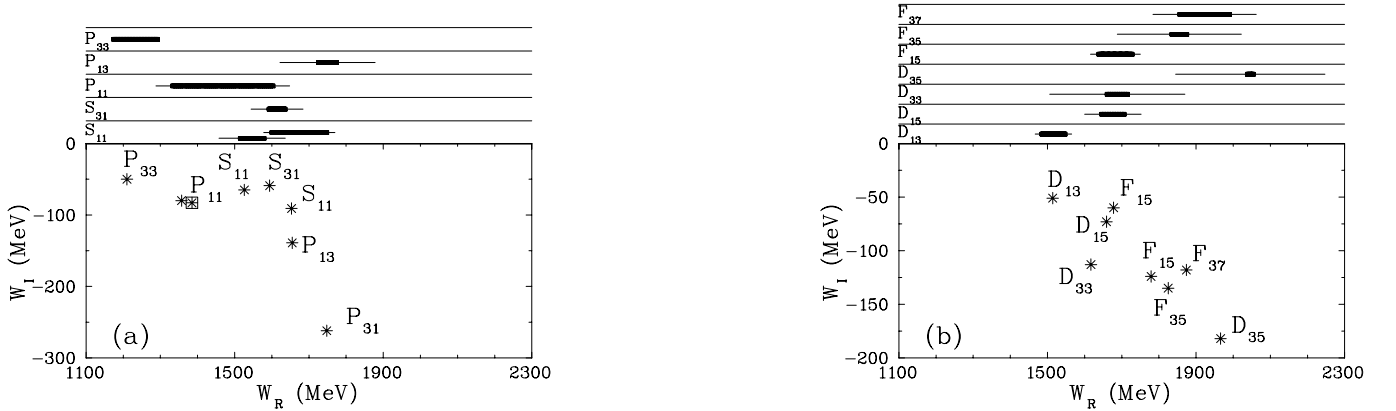


FIG. 9: Comparison of complex plane (bottom panel) and Breit-Wigner (top panel) fits for resonances found in the FA02 solution. Plotted are the result for (a) S- and P-wave resonances and (b) D- and F-wave resonances. Complex plane poles are shown as stars (the boxed star denotes a second-sheet pole). W_R and W_I give real and imaginary parts of the center-of-mass energy. The full (πN partial) widths are denoted by narrow (wide) bars for each resonance.

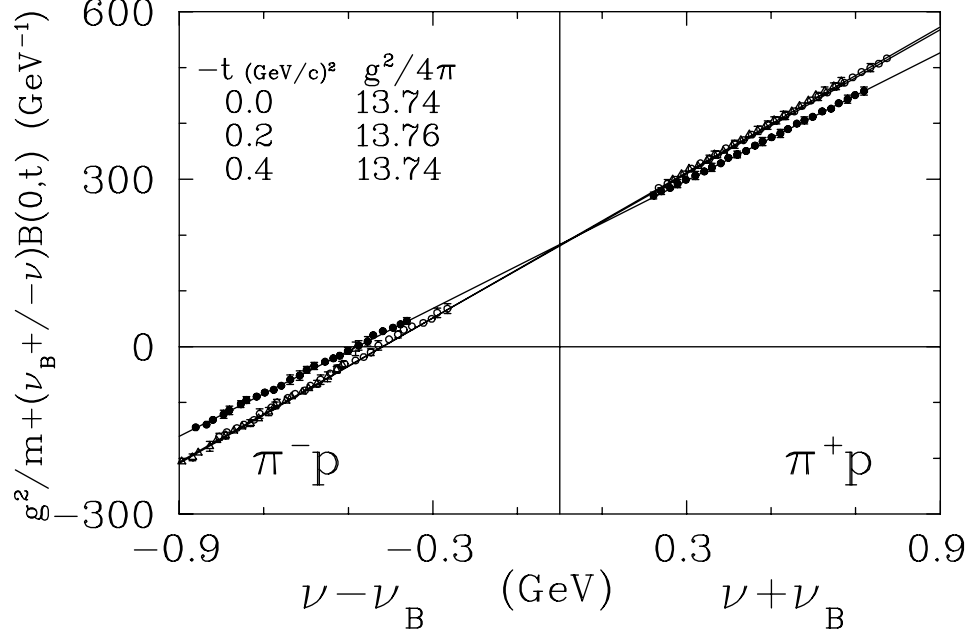


FIG. 10: The Hüper dispersion relation [6] plotted for several values of four-momentum transfer from 0 to -0.4 $(GeV/c)^2$. The y-intercept yields the coupling constant $g^2/4\pi$. Lines represent the least-square averages of individual values.

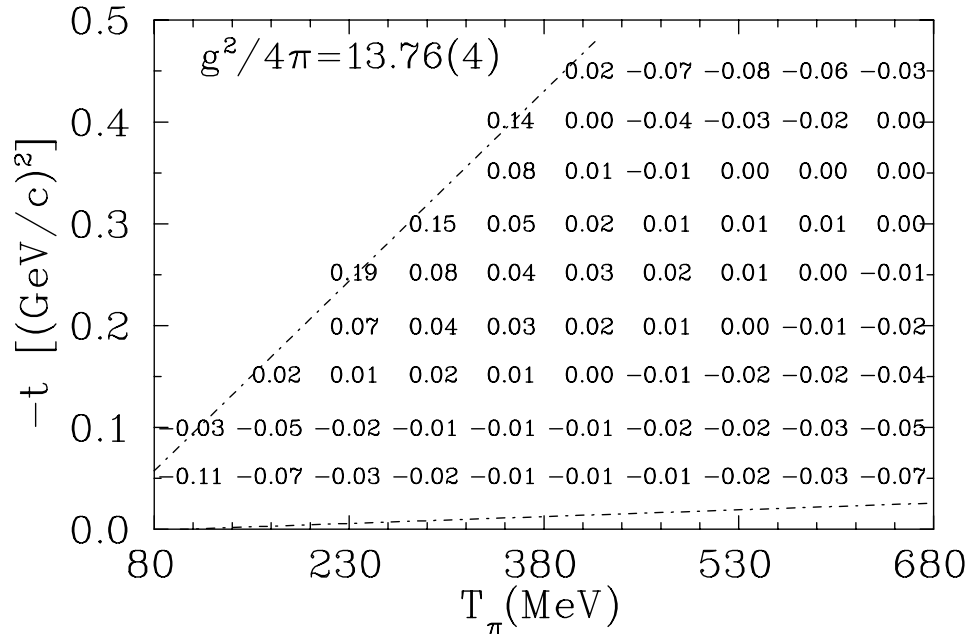


FIG. 11: Deviations from the mean value of $g^2/4\pi$ for FA02 from the $B^+(\nu, t)$ DR evaluated over a grid of T_π and 4-momentum transfer values. Dash-dotted lines show kinematical limits.

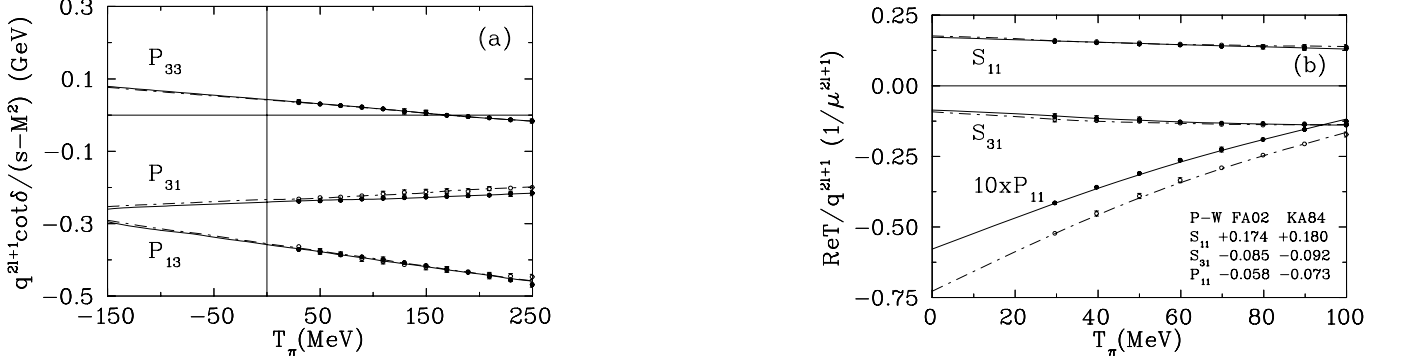


FIG. 12: Plots of (a) $q^{2l+1} \cot \delta / (s - M^2)$ and (b) $\text{Re}T/q^{2l+1}$ for FA02 (solid) and KA84 [54] (dot-dashed) S- and P-wave amplitudes. Scattering lengths (volume) in right panel given in μ^{-1} (μ^{-3}) units. Curves are fits quadratic in T_π .

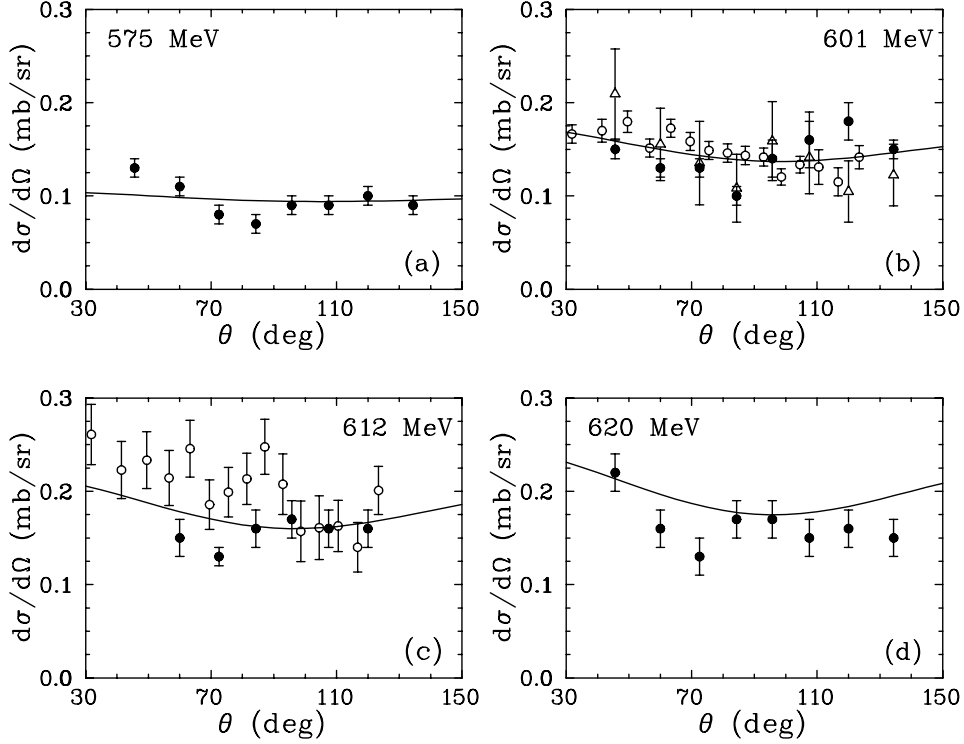


FIG. 13: Differential cross sections for $\pi^- p \rightarrow \eta n$. (a) 575 MeV, (b) 601 MeV, (c) 612 MeV, and (d) 620 MeV. Experimental data are from [34] measurements (filled circles), [38] (open circles), and [39] (open triangles). Solid line shows the FA02 results.

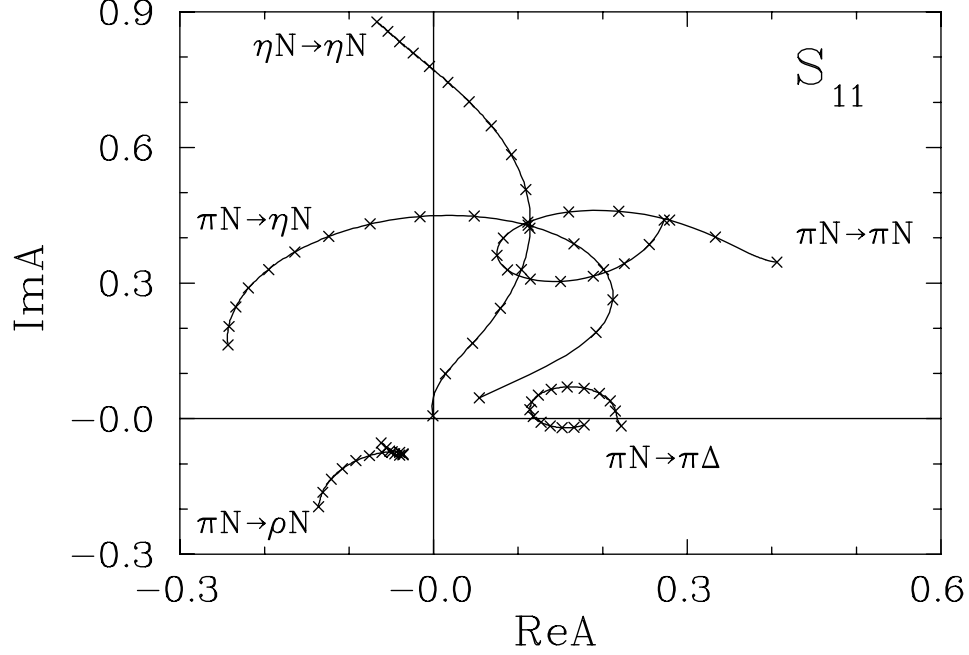


FIG. 14: Essential S_{11} amplitudes from threshold to 800 MeV ($W = 1487$ to 1623 MeV). Crosses indicate every 10 MeV step in W .

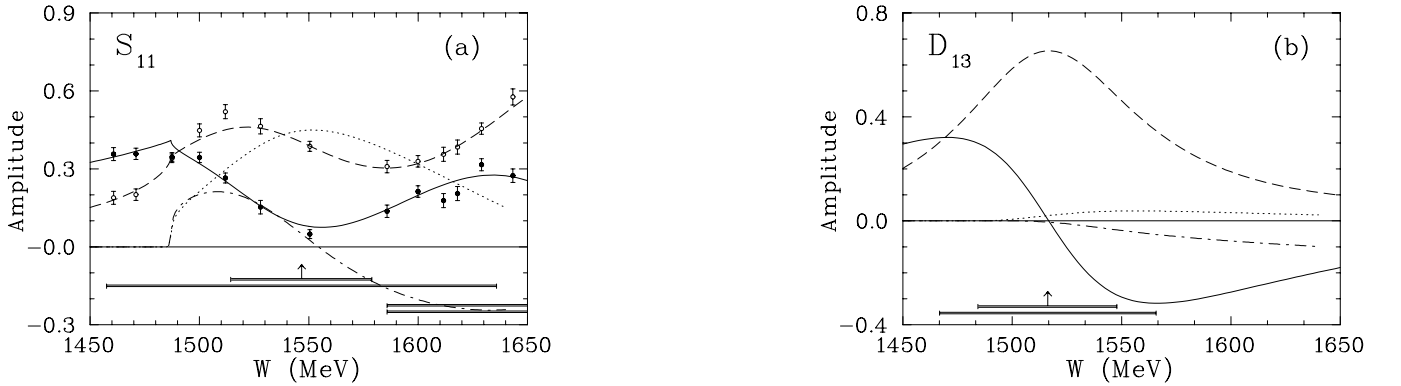


FIG. 15: Low-lying states related to the ηN interaction. Plotted are the results for (a) S_{11} and (b) D_{13} amplitudes. Solid (dashed) curves give the real (imaginary) parts of $\pi N \rightarrow \pi N$ amplitudes, dash-dotted (dotted) curves represent the real (imaginary) parts of $\pi N \rightarrow \eta N$ amplitudes corresponding to the FA02 solution. All amplitudes are dimensionless as in Fig. 6. Vertical arrows indicate W_R and horizontal bars show full $\Gamma/2$ and partial widths for $\Gamma_{\pi N}$ associated with the FA02 results.